universität wien

Diplomarbeit

Genome Release of Human Rhinovirus using Molecular Beacons: an investigation by capillary electrophoresis and fluorescence spectrometry

Matthias Rizzi

angestrebter akademischer Grad

Magister rerum naturalium (Mag. rer. nat.)

Wien 2009

Studienkennzahl lt. Studienblatt	A-419
Studienrichtung lt. Studienblatt:	Chemie
Betreuerin / Betreuer:	Prof. Dr. Ernst Kenndler

Content

I. Introduction 4

I.1 Electrophoresis 4

I.1.1 Theory of electrophoresis 4

I.1.2 Capillary electrophoresis 8

I.1.3 The Electro Osmotic Flow 9

I.2 Molecular Beacon 12

I.2.1 Structure of Molecular Beacons 12

I.2.1.1 Loop sequence 13

I.2.1.2 Stem sequence 13

I.2.1.3 Fluorophore-Quencher Pair 14

I.2.2 Fluorescence Energy Transfer 14

I.2.2.1 Fluorescence resonance energy transfer 15

I.2.2.2 Contact quenching 15

I.3 Human Rhino Virus 16

I.4 Aim of Work 18

II. Experimental section 19

II.1 Reagents 19

II.2 Design of the Molecular Beacon ACGC 19

II.3 Instrumentation and methods 20

II.3.1 Melting characteristics 20

II.3.2 Opening, digestion and hybridization experiments 21

II.3.3 Electrophoretic experiments 22

III. Results and discussion 24

III.1 Melting properties of the Molecular Beacon ACGC 24

III.2 Opening, digestion and hybridization experiments 33

III.3 Capillary Electrophoresis experiments 36

III.3.1 Hybridization experiments on Capillary Electrophoresis 39

IV. Conclusions 42

V. Appendix 44
V.1 Citations 44
V.2 Melting Curves 46
V.3 Electropherograms 47
V.4 Incubation and Opening experiments 50
V.5 List of Abbreviations 51

I. Introduction

I.1 Electrophoresis

I.1.1 Theory of electrophoresis

The principle of electrophoresis is based on migration of ions or ionogenic species in an electric field. Different ions migrate with different velocities in the electric field and can therefore be separated. A cation migrates towards the negatively charged cathode and an anion to the positively charged anode.
The electric field strength, **E**, is given by

$$E = \frac{U}{L}$$

where **U** the voltage applied to the capillary is and **L** the distance between anode and cathode is. A charged particle put into an electric field will first be accelerated by the electric force $\mathbf{k_e}$ (figure I.1.1). The electric force is the driving force for the migration and depends on the charge number **z** of the species, the elementary charge of an electron **e** and the electric field strength **E**.

$$k_e = z \cdot e \cdot E$$

When the ion is accelerated and starts migrating through the solvent, a frictional force will influence the particle. This opposite to the electric force is the friction force $\mathbf{k_\eta}$, which is the product of the velocity **v** of the species and the friction coefficient ***f*.**

$$\mathrm{k}_\eta = v \cdot f$$

The Stokes Law describes the friction coefficient for rigid spherical particles in a continuum:

$$f = 6 \cdot \pi \cdot \eta \cdot r_i$$

where η the dynamic viscosity and $\mathbf{r_i}$ the Stokes' radius of the particle is.
One should mention that the Stokes' radius or hydrodynamical radius is not the cristallographic radius of an ion. It is the radius of the hypothetical solid sphere, which has the same diffusion properties as the particle under consideration.
At the point where steady state is reached, the charged particle migrates with a constant velocity. Both forces set equal lead to the velocity in dependence of the electric field or in other words to the electrophoretic mobility μ:

$$k_e = k_\eta$$

$$v = \frac{z \cdot e \cdot E}{f} \qquad \mu = \frac{v}{E} = \frac{z \cdot e}{f} \quad [m^2/V*s]$$

Looking on the equation for the mobility, we see a dependence of the two variable factors **z**, the charge number of the molecule and ***f***, the friction coefficient which is determined by size and form of the molecule.

The electrophoretic mobility is therefore influenced by three factors, namely:

- charge number *z*
- size
- form of the molecule

We should keep in mind that using the Stokes Law as expression for the friction coefficient is a simplification! It describes the system as a continuum, which means that molecule collisions at molecular dimensions are not taken into consideration.

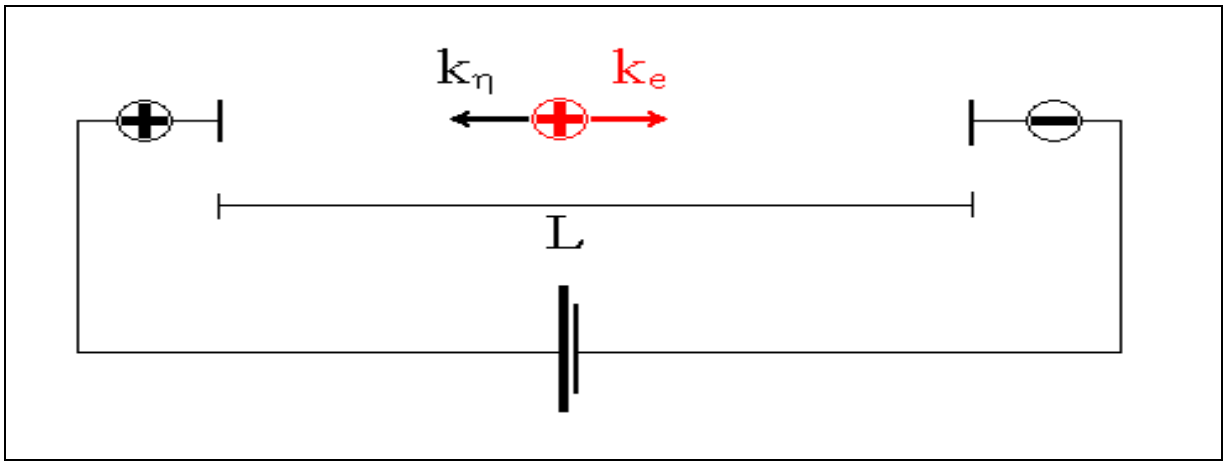

Figure I.1.1: The principle of electrophoresis

So the electrophoretic mobility takes place along the gradient of an electrical potential, like diffusion takes place along a gradient of a chemical potential. It reflects the conductivity of a certain species. The conductivity **κ** however is accessible to us and related to the mobility via:

$$\kappa_i = F \cdot (z_{i,+} \cdot c_{i,+} \cdot \mu_{i,+} - z_{i,-} \cdot c_{i,-} \cdot \mu_{i,-})$$

$$\lambda_i = \frac{\kappa_i}{|c_i|} = F \cdot |z_i| \cdot |\mu_i|$$

Where **F** is the Faraday constant and $\boldsymbol{\lambda_i}$ the molar conductivity.

When we are talking about the electrophoretic mobility, we mean the absolute mobility $\boldsymbol{\mu_{i,0}}$ of a species **i**. The absolute mobility is the mobility of a species at infinite dilution. At this point

there is only one ion in solution. There are no counter-ions which would cause a flow into the opposite direction, so the molecule migrates without being retarded. In this ideal case the molecule has its highest, absolute mobility. One should note at this point that for this approximation the generalized Walden rule is valid:

$$\mu_0 \cdot \eta = const.$$

Of course infinite dilution is hardly to achieve, so in reality we are always dealing with finite solutions of molecules; therefore we introduce the actual mobility $\mu_{i,act}$.:

$$\mu_{i,act} = c_{corr} \cdot \mu_{i,0}$$

which is the product of the absolute mobility and a correction factor c_{corr}. Values for $\mu_{i,0}$ are achieved by extrapolation to zero ionic strength.

For weak electrolytes, which are not completely dissociated, we have to take the dissociation coefficient α_i into account which we derive from the *Henderson-Hasselbach equation* and is given for a monobasic neutral acid with pKa by:

$$\alpha_i = \frac{1}{1+10^{(pKa-pH)}}$$

and reflects the extend of dissociation of a species.
We finally get to the effective mobility.

$$\mu_{i,eff} = \mu_{i,act} \cdot \alpha_i = \mu_{i,0} \cdot c_{corr} \cdot \alpha_i$$

Or in other words:

$$\mu_{i,eff} = \frac{\mu_{i,act}}{1+10^{(pKa-pH)}}$$

for a monovalent acid and

$$\mu_{i,eff} = \sum^{j} \frac{\left(\mu_{j,act} - \mu_{(j-1),act}\right)}{1+10^{(pKa,j-pH)}}$$

for a polyvalent acid.

We now clearly see the importance of the pH value for the effective mobility of a species. To derive reproducible results, it is therefore necessary to work at constant pH values. This is achieved by using buffer systems like borate or phosphate.

We now derived the correct equation for the electrophoretic mobility. But we have not mentioned the reason what this correction factor c_{corr} really is and by what it is influenced.

There are two factors which cause the retardation of the absolute mobility to the actual mobility, the relaxation effect and the electrophoretic effect.

For a better understanding of these two factors let us imagine an ion in solution. When there is no electric field applied, the ion will be surrounded by counter-ions forming a sphere-like "cloud" around it. If an electric field is now applied to the system, the ion will start to migrate out of the center of the cloud and all the counter-ions around it will try to reposition themselves so they form a sphere again. But this process takes a certain relaxation time, after which the center-ion is migrated a bit further. As a result the whole sphere like cloud of counter ions gets deformed limping with its center of charge behind the center ion. Because the charge of the cloud is contrary to the center-ion, it is pulled back. This is the relaxation effect.

The second effect is caused by the movement of the counter-ions opposite to the direction of the center-ion and drag solvent molecules with them. These molecules form a hydrodynamic flow against which the center-ion has to migrate. Hence the center-ion feels a friction force and is retarded. This is the electrophoretic effect.

The quantitative description of the resulting effects is given by the *Debye-Hückel theory*, which combines the *Poisson equation* and the *Boltzmann theorem*. In the end it leads us to the expression of the activity coefficient:

$$\ln \gamma_i = -\frac{z_i^2 \cdot e^2}{8 \cdot \pi \cdot \varepsilon \cdot k \cdot T} \cdot \frac{\kappa}{1 + \kappa \cdot r_i}$$

Where $\boldsymbol{\kappa^{-1}}$ is the Debye-Hückel parameter, which describes the thickness of the ion-atmosphere and has the dimension of a length.

$$\kappa^{-1} = \left(\frac{1000 \cdot \varepsilon \cdot k \cdot T}{8 \cdot \pi \cdot e^2 \cdot N \cdot I} \right)^{\frac{1}{2}} = [m]$$

Where **N** is the Avogadro number and **I** the ionic strength, which is defined by

$$I = \frac{1}{2} \sum c_i \cdot z_i^2$$

This brings us finally to another expression for the actual mobility, the so called *Debye*-Hückel-Onsager equation, which reads in a simplified form:

$$\mu_{act} = \mu_0 - [A \cdot \mu_0 + B] \cdot \sqrt{I}$$

The two Debye-Hückel-Onsager coefficients factors **A** and **B** describe the relaxation effect and the electrophoretic effect. Whereas **A** is a function of the permittivity of the solvent, **B** is a function of the permittivity of the solvent as well as of the viscosity.

Belonging to the electrolyte the experimental data show a very good accordance to the *Debye-Hückel-Onsager theory* for concentrations up to 10^{-3}mol/L.

I.1.2 Capillary electrophoresis

Capillary Electrophoresis (CE) or High Performance Capillary Electrophoresis (HPCE) is the most modern electrophoretic technique. Like in gas chromatography fused silica capillaries with a very small diameter are used. But contrary to chromatographic techniques there is no stationary phase in electrophoresis. The inner diameter of the tube is usually between 25 and 100µm (figure I.1.2). There are also special capillaries with different coatings on the inner side e.g. polyacryamide to reduce the influence of the electro osmotic flow and to increase separation efficiency. The length of these capillaries varies between 20 and 100cm. To reach sufficient separation efficiency it is necessary to apply high voltages between 10 and 30kV (with resulting currents up to 100µA).
One advantage of capillary electrophoresis is the use of very small sample amounts. A capillary of 50cm length and 50µm inner diameter for example has only a volume of 1µL. Therefore sample amounts must not be larger than some nanolitres to reach small injection profiles. Inlet and outlet devices usually have volumes of some hundred microlitres up to some millilitres, whereas the outlet device is always a bit larger.

Injection

There are mainly two ways to inject the sample into the capillary. The first one is done by applying a pressure to inject the sample. The second one is the electrokinetic injection: a high voltage is applied so the sample starts migrating into the capillary either by electrophoresis, by electroosmosis, or by both.

Detection

The detection device is usually placed at the end of the capillary but can be placed in principal at any distance of the capillary. For light based detection it is necessary to have a small window, where the capillary is not coated so a light beam can be focused onto the center.
The most common way of detection in capillary electrophoresis is UV absorption, in addition detection is based on fluorescence, redox reactions and mass spectrometry.
The whole setup for a capillary electrophoresis system can be seen in figure I.1.2.

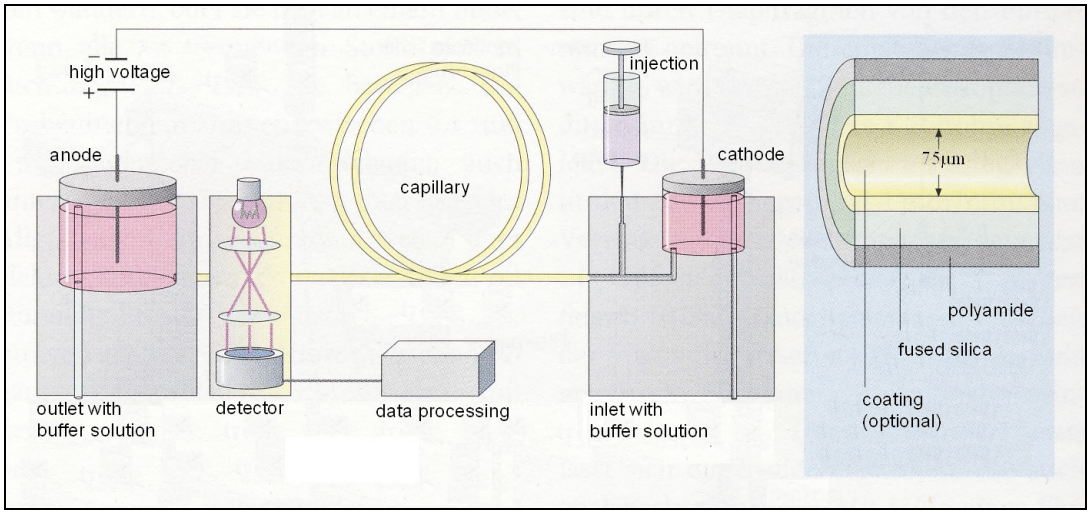

Figure I.1.2: assembly of a capillary electrophoresis system (left) and the profile of a fused silica capillary (right). Figure modified according to figure 9.46, page 458 "Analytische Chemie", Georg Schwedt

I.1.3 The Electro Osmotic Flow

As said before, electrophoresis is the migration of ions and ionogenic species in the electric field. But that is not the whole truth. Also uncharged molecules can migrate within the electric field. This is because of the electro osmotic flow (EOF).
As electro osmotic flow we understand the migration of the whole background solution. The reason for this phenomenon is the formation of a potential on the inner surface of the capillary. In aqueous solutions quartz surfaces tend to be slightly negatively charged.
In solutions with a pH value above 4 this due the deprotonation of terminal silanol groups on the quartz surface. The negatively charged surface attracts mainly cations from the solution, leading to a bilayer. According to the *Gouy-Chapman-Stern-Model* this electric bilayer can be divided into a rigid also called Stern layer and a diffuse layer (figure I.1.3). The Stern layer shows a linear potential-decrease and the diffuse layer an exponential decrease. The height at the beginning of this exponential decreasing potential is also known as ζ-potential and is responsible for the EOF. If an electric field is now applied to the capillary, the positively charged molecules within the diffuse layer start migrating to the negatively charged electrode. The ions beyond the Stern-layer pull solvent molecules with them. As result the whole solutions migrates towards the cathode. The velocity of the EOF is given by the *Smoluchowski eqution*:

$$v_{EOF} = \frac{\varepsilon_0 \cdot \varepsilon_r \cdot \zeta \cdot E}{\eta}$$

Where $\boldsymbol{\varepsilon_0}$ the vacuum permittivity ($8{,}85 \cdot 10^{-12} \cdot J^{-1} \cdot C^2 \cdot m^{-1}$), $\boldsymbol{\varepsilon_r}$ the permittivity of water at 25°C, $\boldsymbol{\zeta}$ the Zeta-potential, **E** the electric field and $\boldsymbol{\eta}$ the viscosity of the solution is.

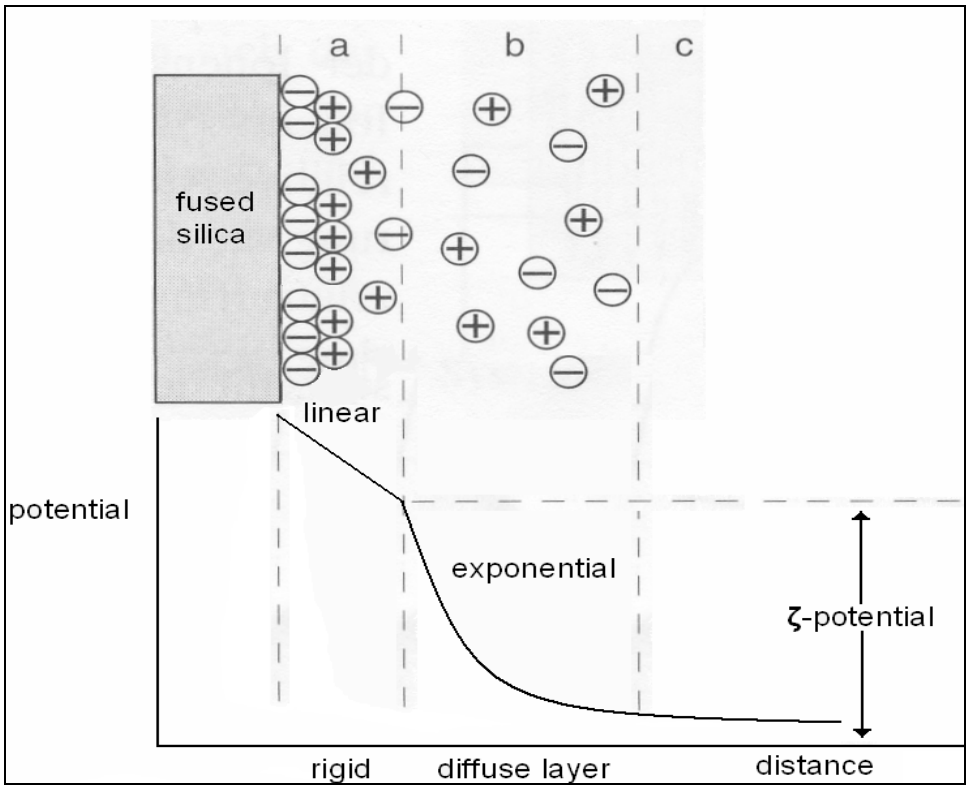

Figure I.1.3: Charge distribution and ζ-potential at the surface of fused silica: the rigid layer (a), the diffuse layer (b) and the bulk (c).

It is hardly possible to eliminate the EOF totally, because there will always be some surface charges. It can only be suppressed by lowering the pH value or using hydrophobic inner coatings.

So positively charged molecules will migrate with the EOF (comigration) and negatively charged ones will migrate against the stream of the solution (contramigration). But if the electrophoretic mobility of an anion is lower than the electrophoretic mobility of the EOF, it will be transported to the cathode anyway (figure I.1.4).

This emerges the possibility by choosing the right properties to separate positively charged molecules as well as negatively charged ones in just one scan. As a result cations will be detected sooner and anions later. Only anions with a higher electrophoretic mobility than the one of the EOF will never reach the detector.

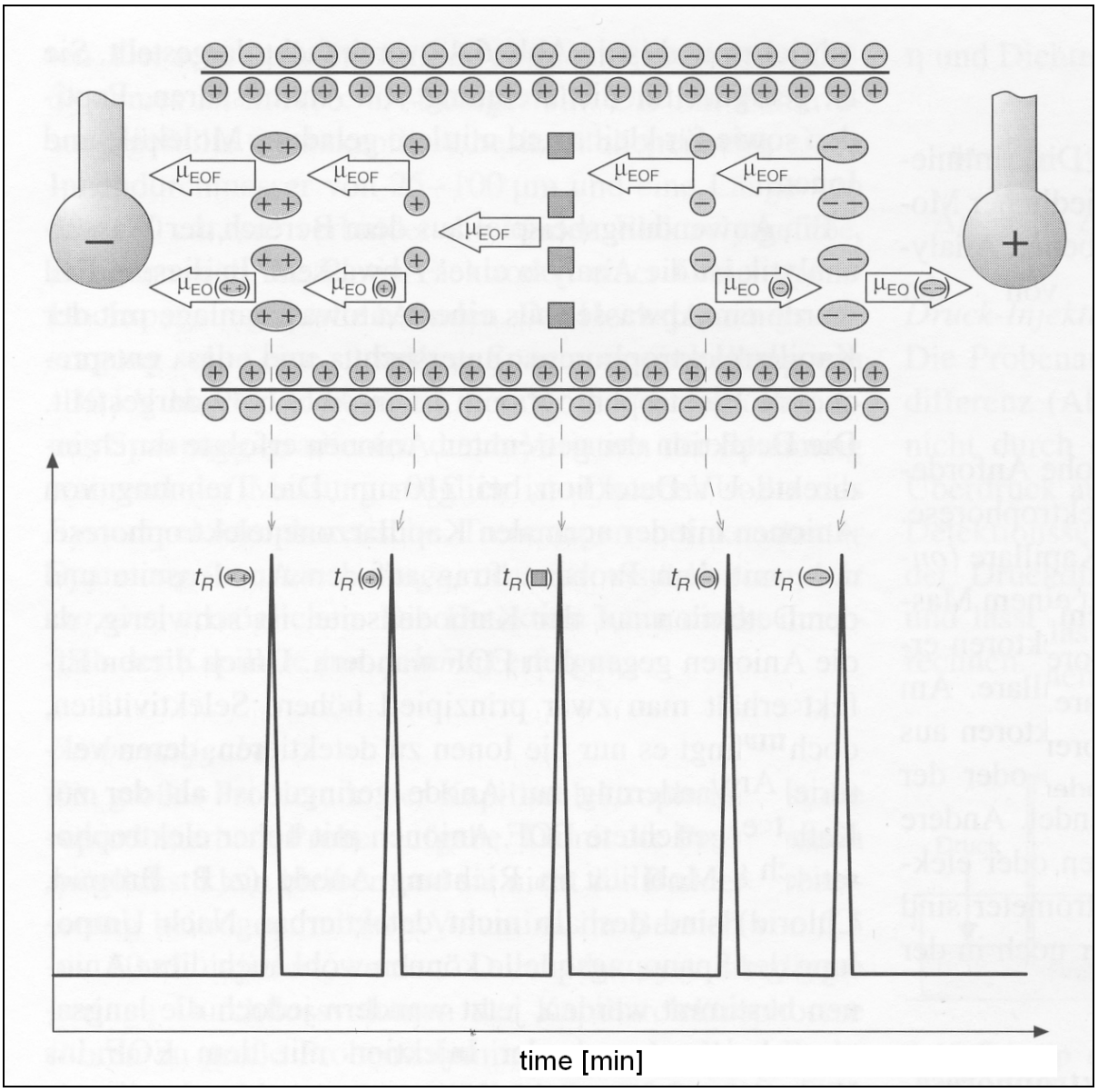

Figure I.1.4: Differential migration of anions and cations overlapping with the EOF. Figure modified according to figure 6.48, page 6-66 "Instrumentelle Analytische Chemie", Karl Cammann.

I.2 Molecular Beacon

The fundamental principle of gene recognition, translation and expression is the hybridization of two complementary oligonucleotide sequences, a process that appears in every living cell. This chemical reaction is extraordinary specific. The molecular Beacon (MB) technique is based on exactly this principle: small fluorescent-labelled probes of single-stranded Desoxyribonucleic Acid (DNA) or Ribonucleic Acid (RNA) fragments hybridize to their complementary sequences in the target. Moreover these probes are not toxic, rather cheap and have a large area of application. Compared to common methods for gene detection, this technique provides great advantages, but research is still in progress.

I.2.1 Structure of Molecular Beacons

A MB is a single-stranded oligonucletide probe with a special loop stem structure (Tyagi and Kramer 1996). It consists of three parts (see figure I.2.1):

- The loop
- The stem
- The fluorophore-quencher pair

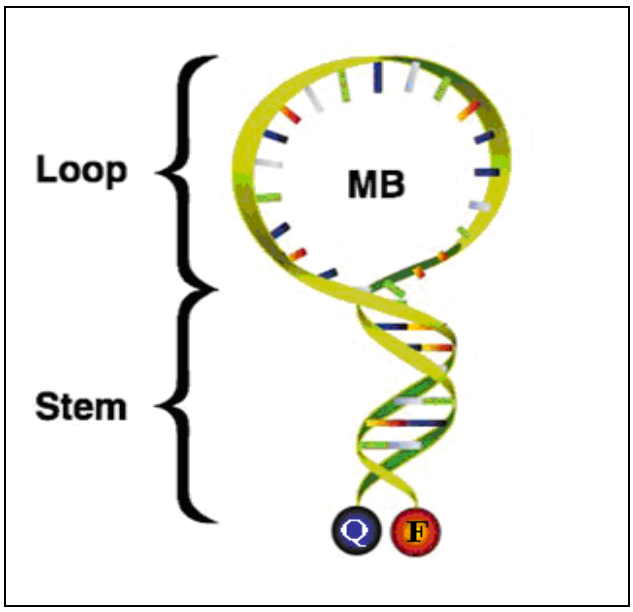

Figure I.2.1: General assembly of a Molecular Beacon probe:
The loop, stem, fluorophore (F) and quencher (Q)

The loop is the actual probe of the Beacon and is complementary to the target sequence. The stem is formed by intramolecular hybridization of complementary sequences, respectively settled at the two ends of the probe sequence. Its stem gives the Beacon its characteristic hairpin structure. To one end of the stem sequence the fluorescent reporter group and to the other the fluorescent quencher group is covalently linked. When the two complementary stem sequences anneal, the whole MB remains dark due to contact-quenching and fluorescence resonance energy transfer of the fluorophore-quencher pair.

I.2.1.1 Loop sequence

The loop sequence is the decisive determinant for the specific working of the whole probe. Its specificity can be adjusted by varying the length of the sequence, whereby the number of nucleotides should be between 15 and 30 pieces (Tyagi and Kramer 1996; Kostrikis, Tyagi et al. 1998; Ortiz, Estrada et al. 1998; Tyagi, Bratu et al. 1998; Bonnet, Tyagi et al. 1999). The longer the sequence is the higher the affinity to its target sequence will be, but the specificity will decrease. It is important that the probe sequence does not form any secondary structure which would hinder the hybridization to the target sequence.

For choosing appropriate probe-target sequences and calculation of their melting temperatures (T_m) commercial software packages like Oligo (Molecular Biology Insight, Inc., Cascade, CO, USA) might be useful.

I.2.1.2 Stem sequence

The stem sequence determines the T_m of the MB, which means the transition from state 2 to state 3 (figure I.2.2). The longer the stem sequence is and the higher its Guanosine and Cytosine amount is the higher the T_m will be. Most basic MB studies (Tyagi and Kramer 1996; Kostrikis, Tyagi et al. 1998; Ortiz, Estrada et al. 1998; Tyagi, Bratu et al. 1998; Bonnet, Tyagi et al. 1999) show that it is appropriate to choose a five to seven base-pairs long stem sequence. A higher stem sequence leads to a better signal to noise ratio but also slows down hybridization kinetics.

A useful tool to predict the T_m of a MB is the DNA folding program by Zuker, free available at http://mfold.bioinfo.rpi.edu/. The program calculates the free energies of formation of secondary structures within nucleic acids and predicts their T_m.

Based on recent studies (Drake and Tan 2004) it is also important to choose the nucleic acid to which the fluorescent dye is linked carefully. The quenching properties of the four different nucleic acids abate in order of G>A>C>T.

I.2.1.3 Fluorophore-Quencher Pair

The number of efficient fluorophore-quencher pairs grew fast in the last decade. The range of emission spectra of fluorescent dyes reaches from the green, e.g. FAM or TET, to the near IR, e.g. LC red 705. A good overview for commercial available fluorophore-quencher pairs and their properties gives the work of Marras (Marras, Kramer et al. 2002; Marras 2006; Marras 2008). Choosing the fluorescent and quenching moiety is of course limited by the instrumental and chemical setup. The selection of the proper fluorphore-quencher pair can improve signal to noise ratio significantly.

I.2.2 Fluorescence Energy Transfer

As already mentioned a MB remains dark in its closed hairpin structure, because fluorescent dye and quenching moiety are in close proximity. The physical mechanism behind this phenomenom is Fluorescence Energy Transfer.

The principle of fluorescence is always the same. The fluorescent dye absorbs energy in form of a photon and is raised from its ground state (S_0) to a higher vibrational level of an excited singlet state (S_x). Then the higher excited vibrational states will return to their ground state by giving away their energy by heat. Only the lowest excited vibrational state (S_1) is able to return to its ground state by emitting light, called fluorescence. The process of excitation takes about one femtosecond, the transitions from higher excited vibrational levels about one picosecond and the transition from S_1 to S_0 takes even one to ten nanoseconds. Because of the "loss" of energy due to heat, the wavelength of the emitted light is always a bit larger than the wavelength of the exciting light.

The fluorescence of a fluorescent dye can be suppressed by another fluorophore or a non-fluorescent dye. This process is called quenching. Two mechanisms are responsible for quenching: contact quenching and fluorescence resonance energy transfer, merged by the umbrella term fluorescence energy transfer. In MB probes always both mechanisms occur.

I.2.2.1 Fluorescence resonance energy transfer

Fluorescence resonance energy transfer (FRET) or Förster type energy transfer is one of the two mechanisms that cause fluorescence quenching. The fluorescent dye or donor emits light

in form of a photon after itself has been excited by absorption of light. The quencher or acceptor absorbs this photon and is excited to a higher vibrational level like the fluorophore before. But instead of emitting light when returning to the ground state, the quencher "looses" its energy due to heat.
Distance between the fluorophore and the quencher as well as the dipole orientations of both molecules are the limiting factors of FRET. FRET is effective in between distances from 1 to 10 nanometres. Of course the emission spectra of the donor must overlap with the absorption spectra of the acceptor so fluorescence quenching can take place.

I.2.2.2 Contact quenching

Contact quenching is also known as ground state complex formation or static quenching. The fluorescent dye and the quencher moiety form a non-fluorescent complex by proton-coupled electron transfer through the formation of hydrogen bonds (Marras 2008). When the complex is excited to a higher vibrational level through absorption of a photon it immediately (after a picosecond) returns to its ground state, unable to emit light.
So the mechanism is basically different compared to FRET, because the fluorophore and the quencher form a complex together. Also the fact that these two molecules change their absorption spectra due to complex formation stands in contrast to FRET.

As already mentioned before, in MB probes always both mechanisms of quenching occur, but not at the same time. In its closed hairpin structure the fluorescent dye and the quencher are in close proximity. The energy transfer occurs directly through contact quenching.
FRET occurs when the Beacon is not closed, but the fluorophore and quencher still come close (1 to 10nm). The efficiency of FRET strongly depends on the choice of the proper fluorophore-quencher pair in regard of the spectral overlap.
In general contact quenching is always more efficient than FRET.

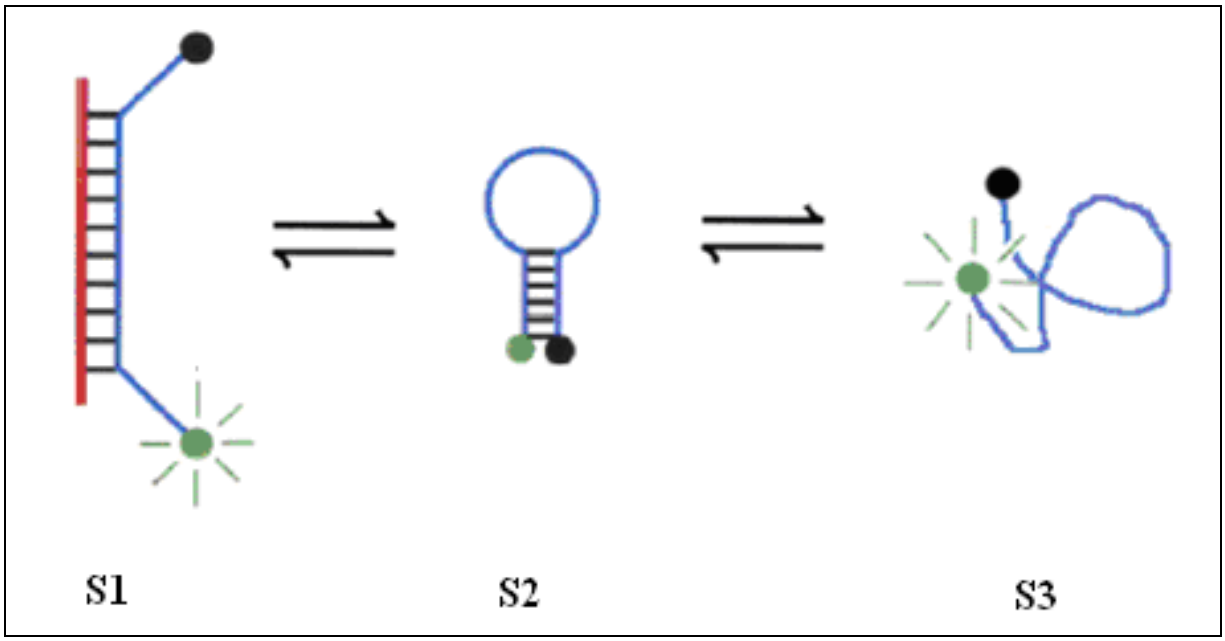

Figure I.2.2: The three possible states of a Molecular Beacon.

S1: The Molecular Beacon is hybridized to its target. The fluorescent dye and the quencher are separated. The result is a high increase of fluorescence compared to state 2.

S2: The Molecular Beacon in its hairpin structure. The Beacon remains closed as no target is available. Therefore the fluorescent dye and the quencher are in close proximity leading to no fluorescence.

S3: The Beacon is opened though no target sequence is available. It is in a random coil structure. Fluorophore and quencher are separated, but fluorescence is not as high as in state 1 due to FRET.

I.3 Human Rhino Virus

Human rhinoviruses (HRV) belong to the family of the Picornaviridae and are the pathogen agent for the common cold in the human body. They are sensitive to acidic environment and prefer temperatures from 33°C to 35°C, which may be a reason why they mostly occur in the nose. The human rhinoviruses consist of two parts, the single-stranded, positive sense, viral RNA and the capsid which forms the shell around the genome. The viral RNA genome is about 7100 nucleotides long having a virus-encoded protein at the 5'-end and a poly-A tail at the 3'-end (Verdaguer, Blaas et al. 2000). The capsid is formed by sixty copies of each of the four viral proteins (VP1, VP2, VP3 and VP4). Whereas the VP1, VP2 and VP3 are exposed at the outer side of the virus surface, VP4 is placed on the inner side of the capsid close to the viral RNA. The whole virus has icosahedral structure with a diameter around 30nm. HRVs are separated into a major and a minor group, belonging to whether they bind to intercellular adhesion molecules 1 (ICAM) or to members of the low density lipoprotein (LDL) receptor family. HRV2, which was used in the present work belongs to the minor group. Its main structural differences to the other human rhinoviruses are located at the internal protein shell surface and at the external antigenic sites (Verdaguer, Blaas et al. 2000). The infection way of the HRV takes place in eight steps: 1) virus binding to its receptors at the plasma membrane; 2) entry into the cell by receptor-mediated endocytosis; 3) conformational change of the virus capsid; 4) release of the viral RNA; 5) RNA penetration into the cytoplasm; 6) synthesis of viral proteins; 7) RNA replication; and 8) assembly and release of new, infectious virions ("Structure-based Study of Viral Replication", edited by R Holland Cheng (University of California, Davis, USA) & Tatsuo Miyamura (The National Institute of Infectious Disease, Japan); chapter I).

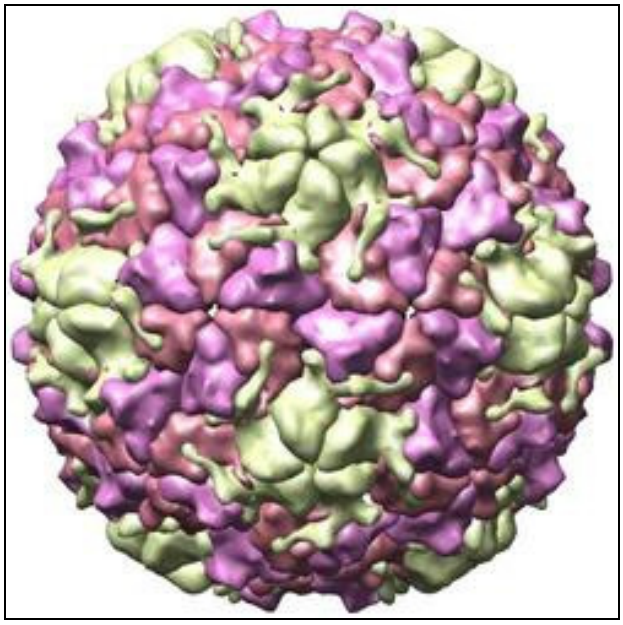

Figure I.3.1: The structure of the human rhinovirus 2 according to (Verdaguer, Blaas et al. 2000).

I.4 Aim of Work

Human Rhinoviruses are one of the initiators of the common cold in the human body. Every year each adult suffers between two and three times from this infections and infants actually thirteen times. HRVs are therefore the cause for one of the most frequent infection of the human body at all, for which reason this family of viruses and its way of infection are studied very intensely. One of the important questions about the way of infection that has not been answered yet clearly is the mechanism of the transfer of the viral RNA from the inner of the virus capsid to the cytosol of the host cell (see section I.3, step 4 and 5 of the infection cycle of the HRV2). There are two possible mechanisms proposed for this transfer. The first one is the virus-induced membrane rupture and the second one is the selective genome translocation across a cellular membrane through pores formed by viral proteins (Prchla, Kuechler et al. 1994).

The present work shall be the groundwork for further studies on this mechanism with a new method of RNA/ DNA recognition, the MB probe. This method firstly described by Tyagi and Kramer (Tyagi and Kramer 1996) became a common tool in real-time Polymerase Chain Reaction (PCR) in the last decade and proves to be a robust tool for DNA/RNA recognition. In the present work design, characterization and application of the MB ACGC are demonstrated. It shall be the first step for further Beacon-based studies on CE in order to reveal the real mechanism of viral RNA transfer.

II. Experimental section

II.1 Reagents

The MB ACGC was purchased by VBC Biotech (Vienna, Austria). The MB consisted of 33 nucleotides, the fluorophore Cy5 at the 5'-end and the Black Hole Quencher (BHQ) at the 3'-end. The MB 's sequence and its closed structure can be seen in figure II.3.1.
Cy5 fluorescent dye dissolved in Dimethylsulfoxide (DMSO) was purchased from Amersham Bioscience (Chafont, England). Poly Adenine 20 nucleotides (PA 20) and Poly Adenine 80 (PA80), both RNA chains with either 20 or 80 Adenine were obtained by VBC Biotech (Vienna, Austria).
HRV2 samples and HRV2 in vitro RNA were prepared by Irene Gösler. Boric acid (analytical grade), Magnesium chloride (as $MgCl_2*6H_2O$, analytical grade) and sodium hydroxide (pure pellets) were obtained from Merck (Darmstadt, Germany). Dimethylsulfoxid, dried SeccoSolv® (max. 0,025% H_2O) was also purchased from Merck.
For Ribonuclease (RNase) free working a Ribonucleoside-vanadyl complex was obtained from New England Biolabs® Inc. (Beverly MA 01915, USA). Desoxyribonuclease I (DNase I) and DNase I reaction buffer were both ordered from New England Biolabs® Inc.
For CE experiments all samples were membrane filtered and degassed before injection.
For all experiments containing viral RNA the samples had to be prepared very carefully to prevent the samples contaminated with RNase. Therefore pipette tips and also reaction vials had been washed with EtOH before they were used.

II.2 Design of the Molecular Beacon ACGC

The MB ACGC (MB ACGC, figure II.3.1), named after its stem sequence was designed to detect the RNA of the Human Rhinovirus 2 (HRV2). The thermodynamic calculations of the MB ACGC were carried out with the free available T_m and 2-state hybridization server by Zuker (http://mfold.bioinfo.rpi.edu/). The T_m–server allowed us to calculate the melting properties of the MB ACGC in dependence of the concentrations of Na^+ and Mg^{2+} and its Gibbs energy, whereby the 2-state hybridization server the same for the probe-target-hybrid did. All details for the thermodynamic calculations with the DINAMelt Server Prediction can be seen in the section III.1, table III.1.1-III.1.6.

Because there was no need for a high T_m of the present MB like in PCR an only four nucleotide long stem sequence was chosen with an Adenine next to the fluorophore at the 5'-end to minimize quenching due to FRET induced by nucleotides (Torimura, Kurata et al. 2001).
In order to have a simple but effective tool, as target sequence the poly-A tail in the viral genome (Gerber, Wimmer et al. 2001) was chosen. Because of the weaker binding between Adenine and Thymine/Uracil compared to Guanine and Cytosine the poly-A tail is more likely to be freely available for binding and therefore preferable to other regions. The length of the target sequence was according to Tyagi and Kramer for optimum sequence length chosen to be 25 nucleotides long.
The fluorophore-quencher pair was chosen to be Cy5 at the 5'-end and the BHQ at the 3'-end according to former studies on optimum fluorophore quencher pairs (Marras, Kramer et al. 2002; Marras 2006; Marras 2008) and the instrumental setup.

II.3 Instrumentation and methods

II.3.1 Melting characteristics

For Characterization of the MB ACGC, melting curves were measured on the iQ5 Real-Time PCR Detection System (iCycler) from BioRad. Special thanks to Prof. Cichna-Markl and her working group for providing the instrument. All data was collected and analysed with the CFX-Manager by BioRad.
Melting curves were taken from 25°C up to 95°C in 0.5°C steps, lasting 30 seconds at each temperature step in the beginning. Lateron the temperature steps were increased up to 1°C with one minute lasting at each step without any significant change of the melting curves. The total volume of each sample was 25µl and the concentration of the MB was always 100nM. For each sample a threefold onset was prepared, each separately and measured three times to check the reversibility of the conformational change of the MB.
For determining the T_m of the MB also the quenching of the fluorescent dye due to FRET induced by heat had to be taken into account. Therefore melting curves of the fluorophore Cy5 in the same solution and concentration like the MB were taken and subtracted from the signal of the MB. The T_m of the Beacon was finally calculated by applying tangents to the

linear domains of the Cy5 corrected melting curves. The intersection of the two tangents was the T_m of the MB.
For developing a proper method for CE experiments, melting curves of the MB in following background solutions were done: H_2O, 30mM borate buffer, 30mM borate buffer with 0,10mM $MgCl_2$, 30mM borate buffer with 1,00mM $MgCl_2$, 50mM borate buffer, 100mM borate buffer, 100mM borate buffer with 0,10mM $MgCl_2$ and 100mM borate buffer with 1,00mM $MgCl_2$. The pH of all samples but water was set to 8.3.

II.3.2 Opening, digestion and hybridization experiments

Hybridization, opening and digestion measurements of the MB were carried out on the Perkin Elmer Victor 3 1420 Multilaber Plate Reader. For excitation a continuous wavelength (CW) lamp filter for 590nm and for detection a CW lamp filter for 650nm was used. The wavelength window had a width of 15 nanometers. For measurements a 96-well plate was used. Each sample had a total volume of 100µl and a total MB concentration of 100nM.
The digestion and opening experiments were done to check the highest expectable fluorescence signal of the MB ACGC. For digestion with DNase I, the DNase I reaction buffer was used with a total concentration of 10 mM Tris-HCl with 2.5 mM $MgCl_2$ and 0.5 mM $CaCl_2$. The incubation at 37°C took place for about 15 minutes, the pH was set to 8.3.
In order to have a tool to open the MB without digesting it, EDTA in different concentrations reaching from 20nM up to 1µM was used (table V.5.1).
For hybridization experiments, the MB was incubated together with the poly-Adenine 20 (Poly-A), poly-A 80 and the native HRV2, all three targets in excess. All samples were heated up to 56°C for 15 minutes, cooled down and measured at 25°C. The sample buffer was 30mM borate buffer with 1,00mM $MgCl_2$, pH 8.3. The concentration of the HRV2 was 10-50µg/ml according to its preparation.

II.3.3 Electrophoretic experiments

Electrophoretic experiments were carried out on the Agilent Capillary Electrophoresis (CE) instrument with on board UV detection coupled with a Picometrics ZETALIF Evolution, Laser Induced Fluorescent Detector (LIF-Detector). Separation took place in a fused silica capillary, all capillary parameters can be seen in table II.3.1. An external Helium-Neon (HeNe) laser from Melles Griot (maximum at λ_{ex} 594nm) was used. For optimum detection the LIF-Detector was equipped with a cut-off emission filter block for red light (for all wavelengths above λ = 620nm). All data from the CE was collected and evaluated with the HPCHEM Software by Hewlett Packard®.
The detection of the MB was assured by the LIF-detector and identification of the viral compounds was achieved by UV detection. Determination between viral RNA and virus proteins was achieved by comparing the continuous spectra. Viral RNA has a maximum at 260nm, whereas virus proteins do not (continuous UV-spectra and the migration profile of Dimethylsulfoxide, virus protein and viral RNA can be seen in electropherogram III.3.1).
As background electrolyte 30mM borate buffer (bb) was used, the sample buffer always was 30mM borate buffer with 1,00mM $MgCl_2$, both at pH 8.3. Sample volumes differed from 20 up to 100µl. The capillary was flushed with 30mM borate buffer for two minutes before each run and with 1M NaOH and H_2O bidest. for two minutes afterwards. The applied voltage was +20kV and the capillary was thermostated to 25°C.

Table II.3.1: capillary parameters		
total length	73,0	cm
length to UV-window	23,5	cm
length to fluorescent detection	58,0	cm
inner diameter	75,0	µm

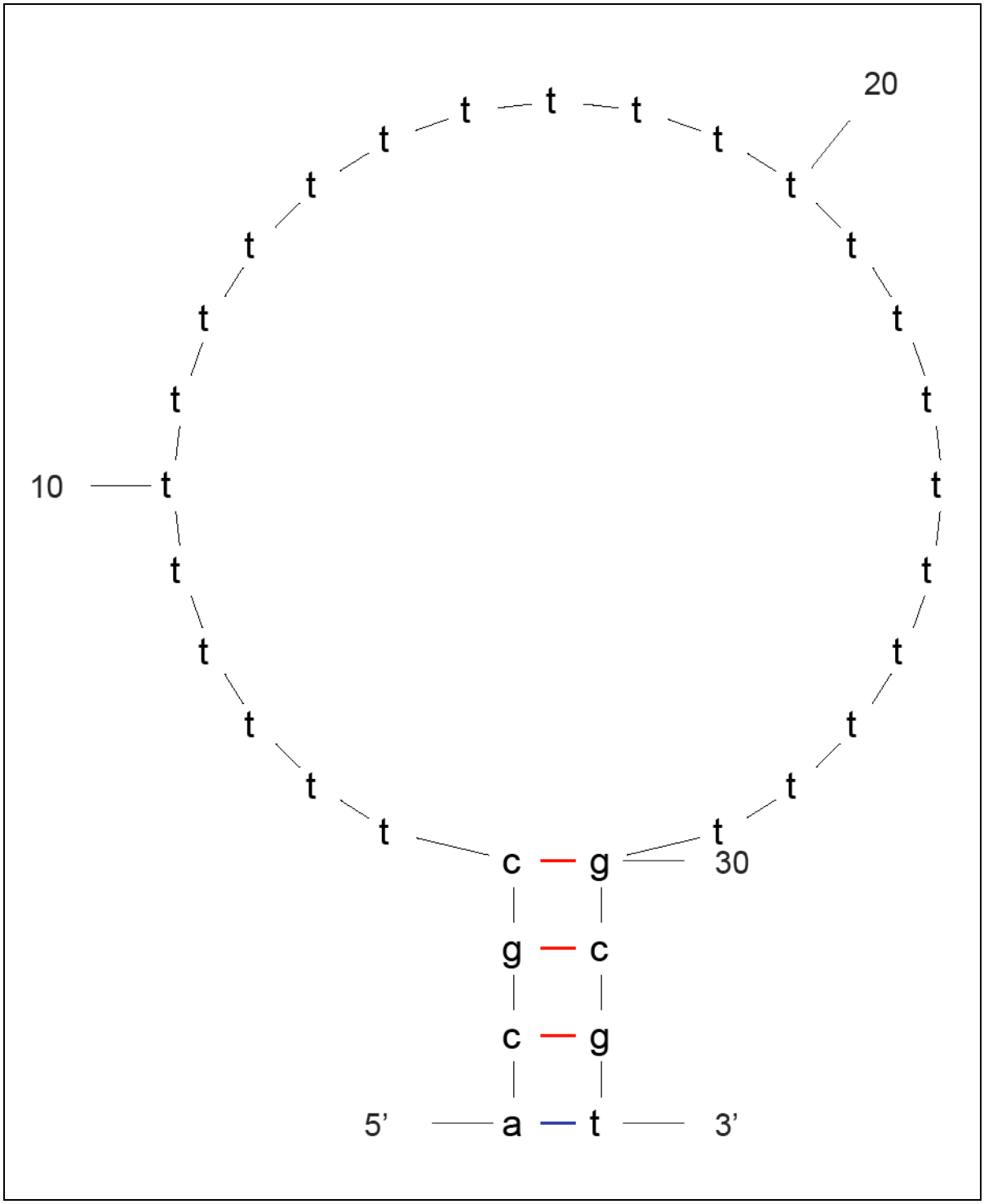

Figure II.3.1: Molecular beacon "MB ACGC" in its closed form purchased from VBC Biotech (Vienna, Austria), with Cy5 at the 5'-end and BHQ at the 3'-end.

III. Results and discussion

III.1 Melting properties of the Molecular Beacon ACGC

The purpose of determining the melting properties was firstly to verify the reversibility of the transition from the Beacons hairpin structure to its opened structure (see Figure I.2.2, transition from S2 to S3) and secondly to check the influence of $MgCl_2$ and different concentrations of borate buffer on the melting behaviour of the MB.
To check if the MB really returns to its closed ground state, the hairpin structure, after it was opened, melting curves of one sample were repeated after a time delay of 15 minutes to allow the sample to cool down (see melting curve III.1.1). In case of a partial or total irreversibility the fluorescence signal of the second run at the starting temperature would be much higher than the signal of the first run, because MB is still opened and fluoresces. A total irreversibility would then show a linear decrease to higher temperatures. A partial irreversibility would still have the form of a melting curve but much more plain than its previous run.

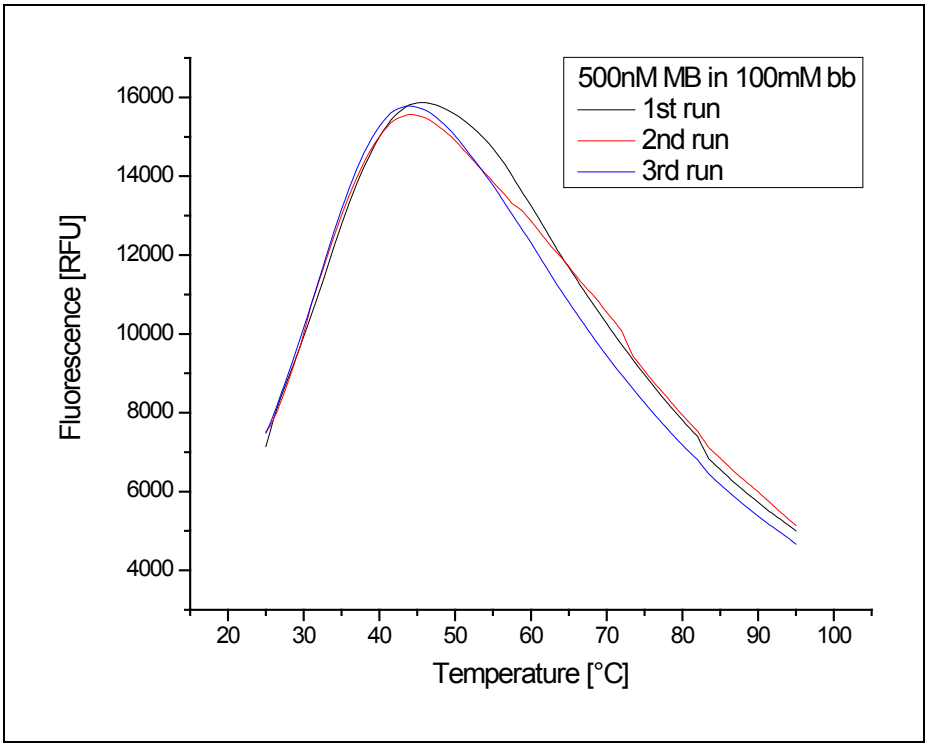

Melting curve III.1.1: Reversibility of the transition from the Beacons closed structure S2 to its opened structure S3 (compare to Figure I.2.2). Same sample of 500nM MB in 100mM bb measured three times in a row with 15 minutes in between each run. The change of the fluorescence signal at the starting temperature 25°C is less than 5 % and less than 3% at their signal maxima after three runs.

The further characterization of the MB revealed a large discrepancy between calculated melting properties by the T_m-server by Zuker and our experimental data. Especially the influence of the Mg^{2+} concentration but also the Na^+ concentration of the buffer solution in general on the T_m was much higher than expected.

In table III.1.1 – III.1.3 the values calculated by the T_m-server by Zuker for 100nM MB ACGC in 30mM bb, 30mM bb with 0,10mM $MgCl_2$ and for 30mM bb with 1,00mM $MgCl_2$ can be seen. Melting curves III.1.2 - III.1.4 show the melting plots for same concentrations and their resulting T_m. In Figure III.1.3 & III.1.4 the computed structures of the MB ACGC hybridized to its target and in its hairpin-structure can be seen.

Job Parameters		calculated values for closed MB		
	conc. [mM]	ΔG	-0,9	kcal*mol^{-1}
Target-sequence	100	ΔH	-36,4	kcal*mol^{-1}
Na^+	30	ΔS	-119,2	kcal*K^{-1}*mol^{-1}
Mg^{2+}	0	T_m	32,1	°C
		calculated values for probe-target-hybrid		
		ΔG	-19,4	kcal*mol^{-1}
		ΔH	-186,6	kcal*mol^{-1}
		ΔS	-560,8	kcal*K^{-1}*mol^{-1}
		T_m	45,0	°C

Table III.1.1: calculated values for MB ACGC in 30mM bb

Job Parameters		calculates values for closed MB		
	conc. [mM]	ΔG	-1,1	kcal*mol^{-1}
Target-sequence	100	ΔH	-36,4	kcal*mol^{-1}
Na^+	30	ΔS	-118,4	kcal*K^{-1}*mol^{-1}
Mg^{2+}	0,10	T_m	34,2	°C
		calculated values for probe-target-hybrid		
		ΔG	-21,4	kcal*mol^{-1}
		ΔH	-190,7	kcal*mol^{-1}
		ΔS	-567,9	kcal*K^{-1}*mol^{-1}
		T_m	48,2	°C

Table III.1.2: calculated values for MB ACGC in 30mM bb with 0,10mM $MgCl_2$

Job Parameters		calculated values for closed MB		
	conc. [mM]	ΔG	-1,3	kcal*mol^{-1}
Target-sequence	100	ΔH	-36,4	kcal*mol^{-1}
Na^+	30	ΔS	-117,6	kcal*K^{-1}*mol^{-1}
Mg^{2+}	1,00	T_m	36,4	°C
		calculated values for probe-target-hybrid		
		ΔG	-23,5	kcal*mol^{-1}
		ΔH	-190,7	kcal*mol^{-1}
		ΔS	-560,9	kcal*K^{-1}*mol^{-1}
		T_m	52,0	°C

Table III.1.3: calculated values for MB ACGC in 30mM bb with 1,00mM $MgCl_2$

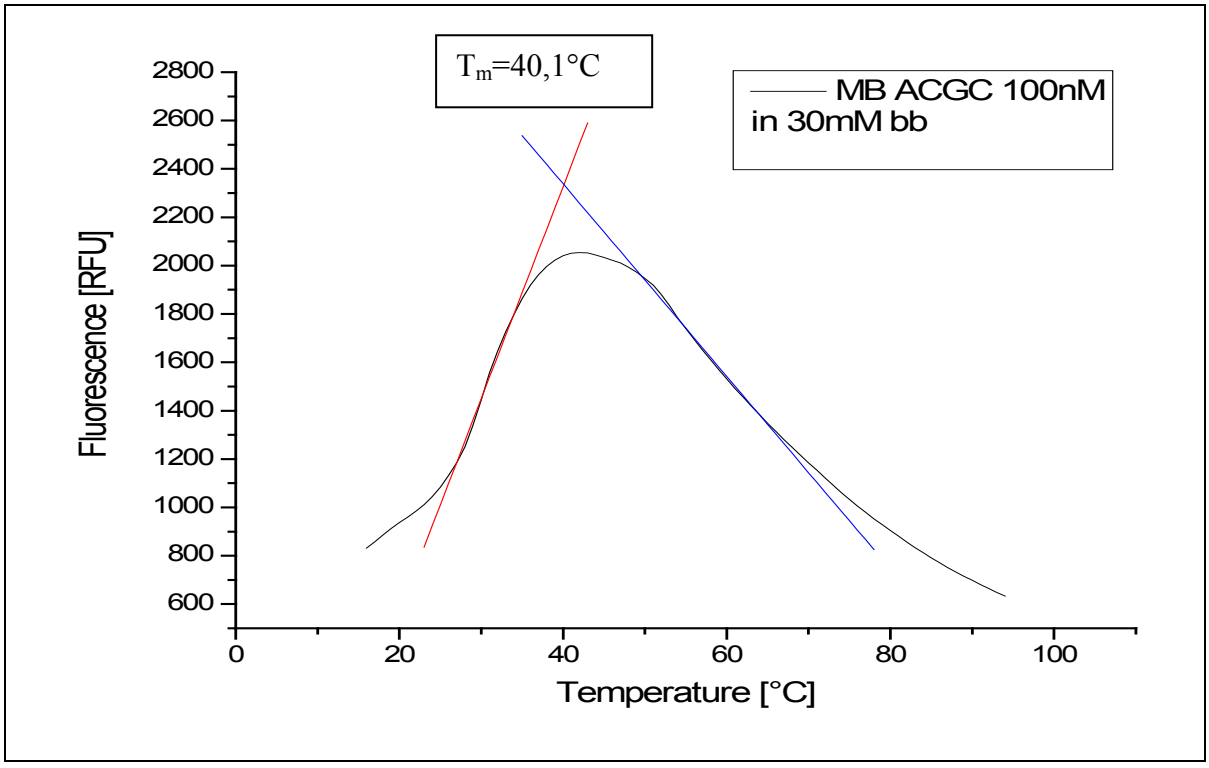

Melting curve III.1.2: 100nM MB ACGC in 30mM bb

tangents: y = 87,7x - 1180 and y = -39,8x + 3930; resulting Tm=40,1°C for

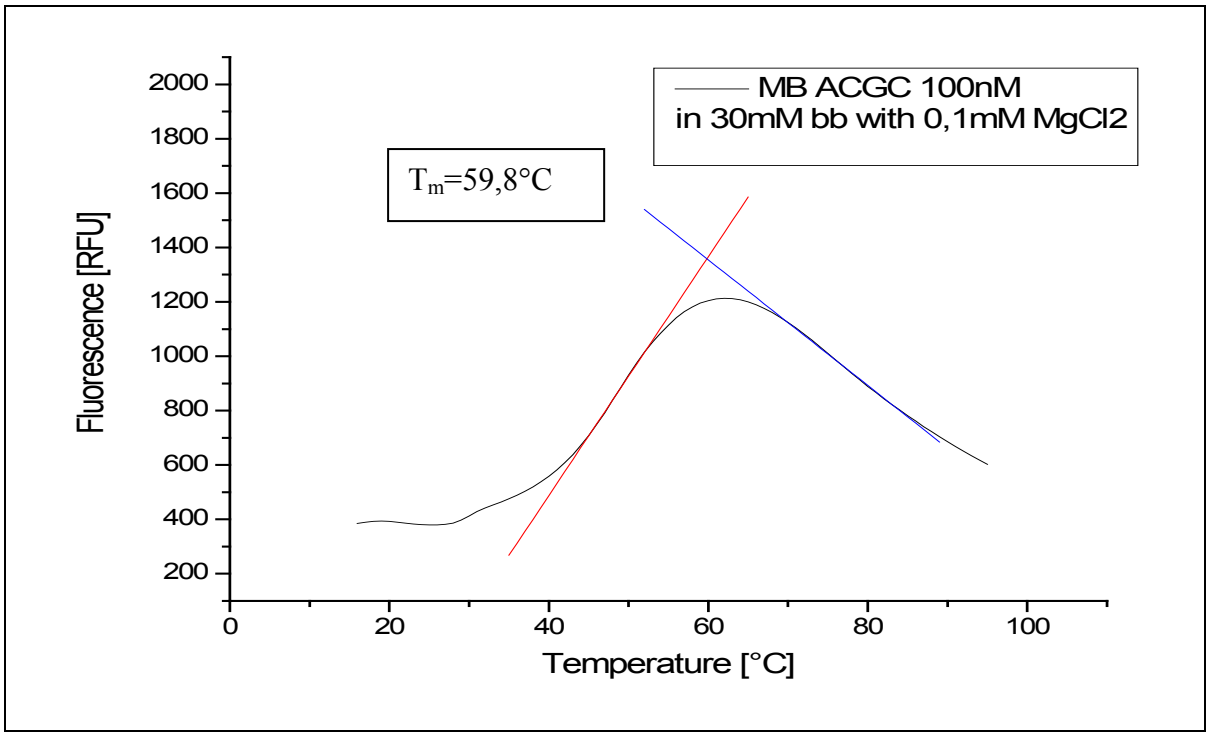

Melting curve III.1.3: 100nM MB ACGC in 30mM bb with 0,10mM $MgCl_2$

tangents: y = 43,9x – 1270 and y = -23,1x + 2740; resulting Tm=59,8°C

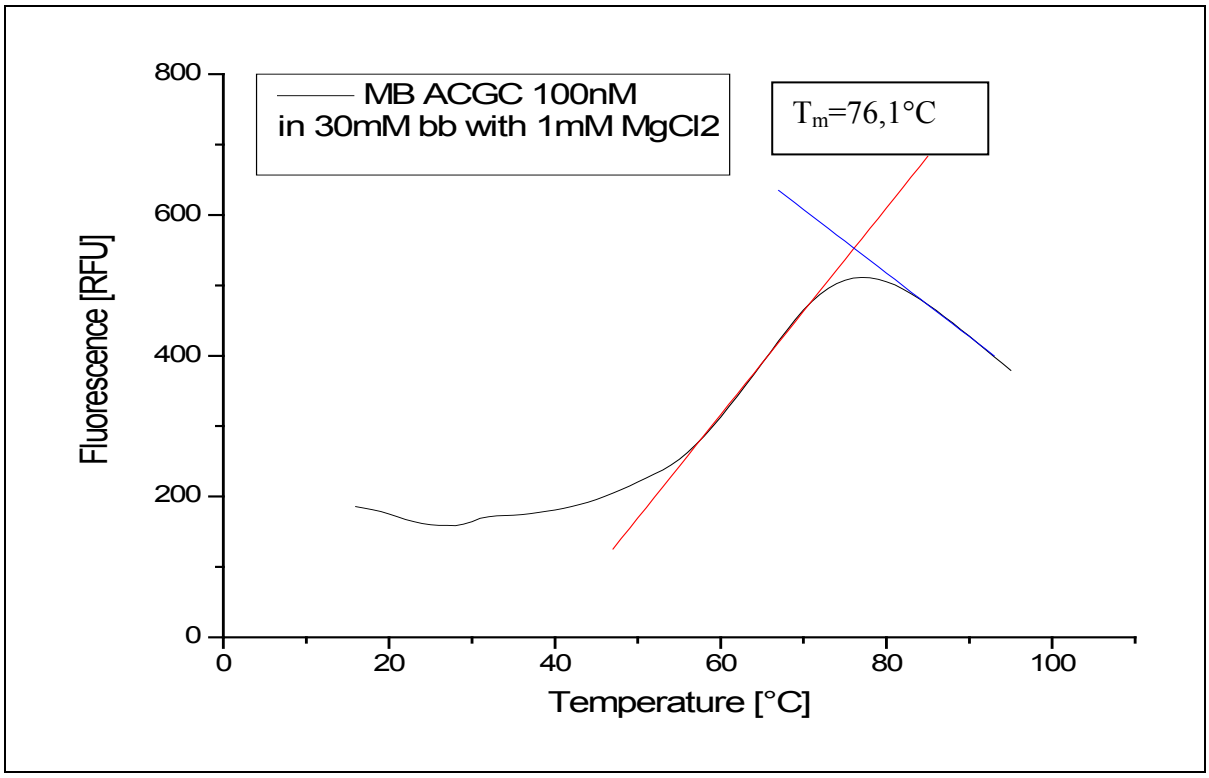

Melting curve III.1.4: 100nM MB ACGC in 30mM bb with 1,00mM $MgCl_2$

tangents: y = 14,6x - 564 and y = -9,03x + 1240; resulting Tm=76,1°C

The calculated stem T_m for the MB ACGC in a 30mM borate buffer solution was 32.1°C, whereas the experimental result was 40.1°C, a difference of 8.0°C. With higher concentrations of Mg^{2+} the difference gets even larger. The calculated T_m for the MB ACGC in 30mM bb with 0,10mM $MgCl_2$ was 34.2°C, instead the experimental result provided a stem T_m of 59.8°C and for the MB in 30mM bb with 1,00mM $MgCl_2$ the calculated T_m was 36.4°C versus the experimental result of 76.1°C, almost 40°C higher than expected. Figure III.1.1 shows the calculated and experimental T_m in dependence of the Mg^{2+} concentration.

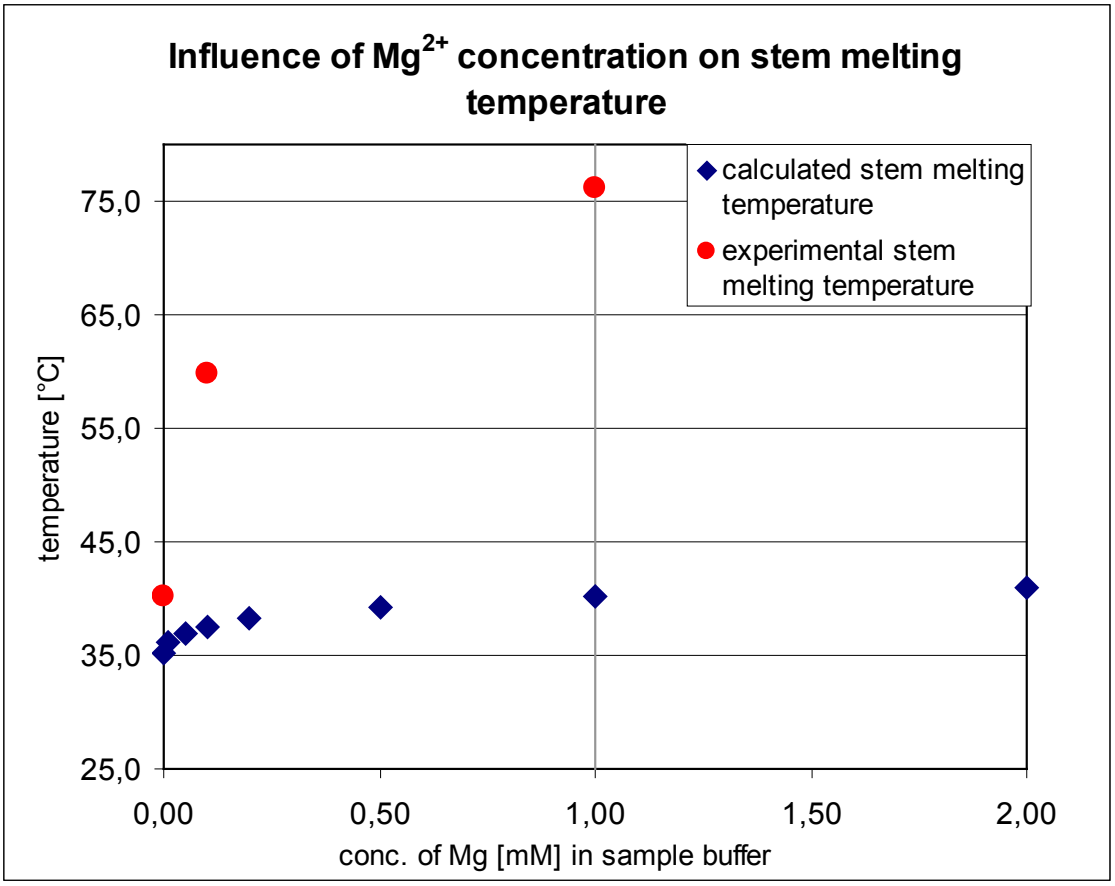

Figure III.1.1: Calculated (with T_m-server by Zuker) and experimental values for the stem melting temperature of the MB ACGC in 30mM borate buffer with different concentrations of $MgCl_2$.

The influence of the Na^+ concentration in the buffer solution was much smaller, but still significant. The calculated T_m for the MB ACGC in 30mM bb, 50mM bb and 100mM bb were 35.1°C, 36.7°C, and 39.1°C (see table III.1.4 – III.1.6), whereas the experimental values for same bb concentrations were 41.1°C, 45.3°C and 49.7°C (see melting curve III.1.5 – III.1.7). In figure III.1.2 the difference between the calculated and experimental T_m in dependence of the Na^+ concentration are plotted.

Job Parameters		calculated values for closed MB		
	conc. [mM]	ΔG	0,2	kcal*mol^{-1}
Target-sequence	0,001	ΔH	-31,9	kcal*mol^{-1}
Na^+	30	ΔS	-103,5	kcal*K^{-1}*mol^{-1}
Mg^{2+}	0	T_m	35,1	°C
		calculated values for probe-target-hybrid		
		ΔG	-12,6	kcal*mol^{-1}
		ΔH	-186,6	kcal*mol^{-1}
		ΔS	-560,9	kcal*K^{-1}*mol^{-1}
		T_m	45,0	°C

Table III.1.4: calculated values for MB ACGC in 30mM bb

Job Parameters		calculated values for closed MB		
	conc. [mM]	ΔG	0,02	kcal*mol^{-1}
Target-sequence	0,001	ΔH	-31,9	kcal*mol^{-1}
Na^+	50	ΔS	-102,9	kcal*K^{-1}*mol^{-1}
Mg^{2+}	0	T_m	36,7	°C
		calculated values for probe-target-hybrid		
		ΔG	-14,1	kcal*mol^{-1}
		ΔH	-186,6	kcal*mol^{-1}
		ΔS	-556,3	kcal*K^{-1}*mol^{-1}
		T_m	-47,5	°C

Table III.1.5: calculated values for MB ACGC in 50mM bb

Job Parameters		calculated values for closed MB		
	conc. [mM]	ΔG	-0,2	kcal*mol^{-1}
Target-sequence	0,001	ΔH	-31,9	kcal*mol^{-1}
Na^+	100	ΔS	-102,2	kcal*K^{-1}*mol^{-1}
Mg^{2+}	0	T_m	39,1	°C
		calculated values for probe-target-hybrid		
		ΔG	-16	kcal*mol^{-1}
		ΔH	-186,6	kcal*mol^{-1}
		ΔS	-550	kcal*K^{-1}*mol^{-1}
		T_m	51,0	°C

Table III.1.6: calculated values for MB ACGC in 100mM bb

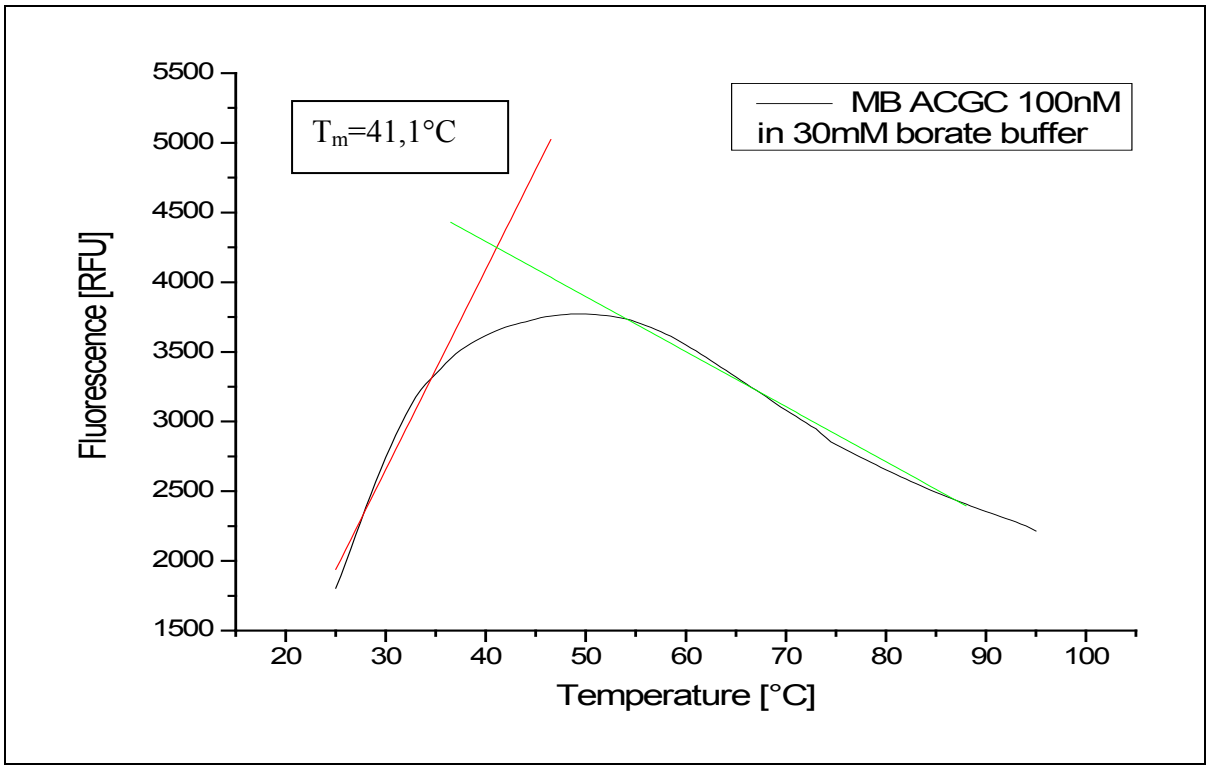

Melting curve III.1.5: 100nM MB ACGC in 30mM bb

tangents: y = 144x - 1650 and y = -39,5x + 5870; resulting Tm=41,1°C

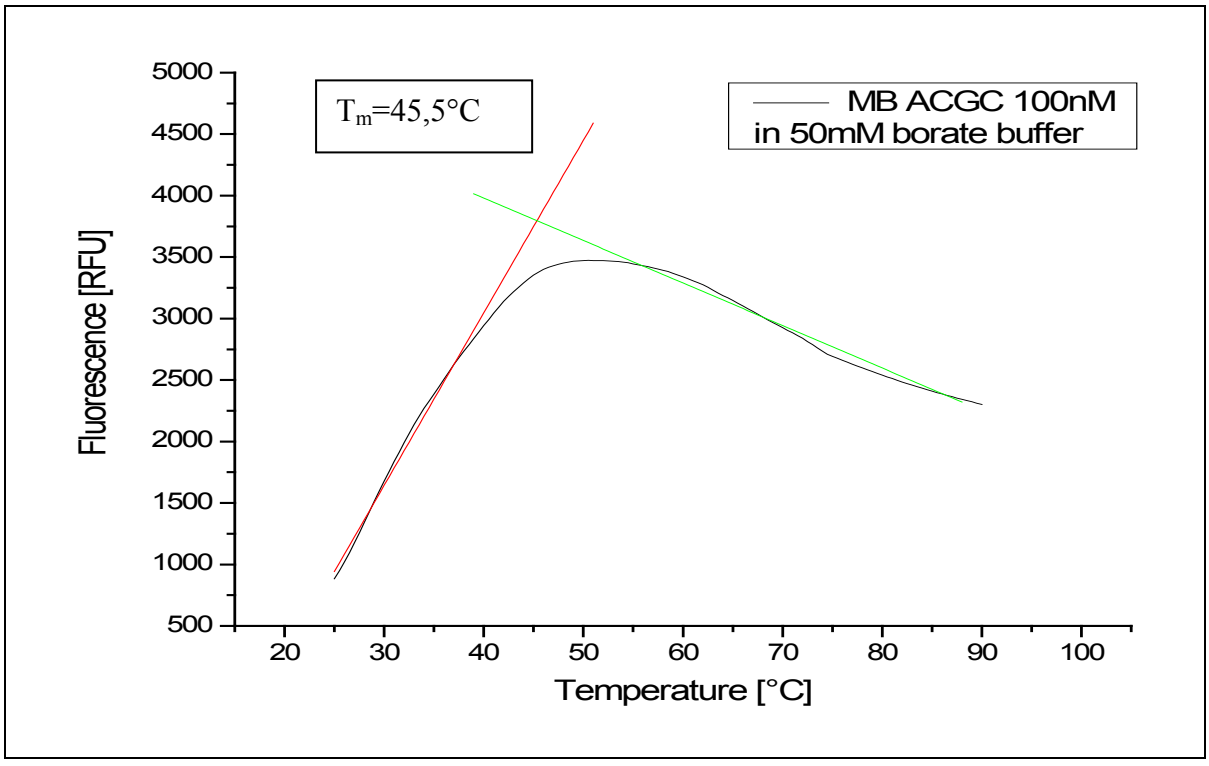

Melting curve III.1.6: 100nM MB ACGC in 50mM bb

tangents: y = 140x - 2560 and y = -34,5x + 5360; resulting Tm=45,4°C

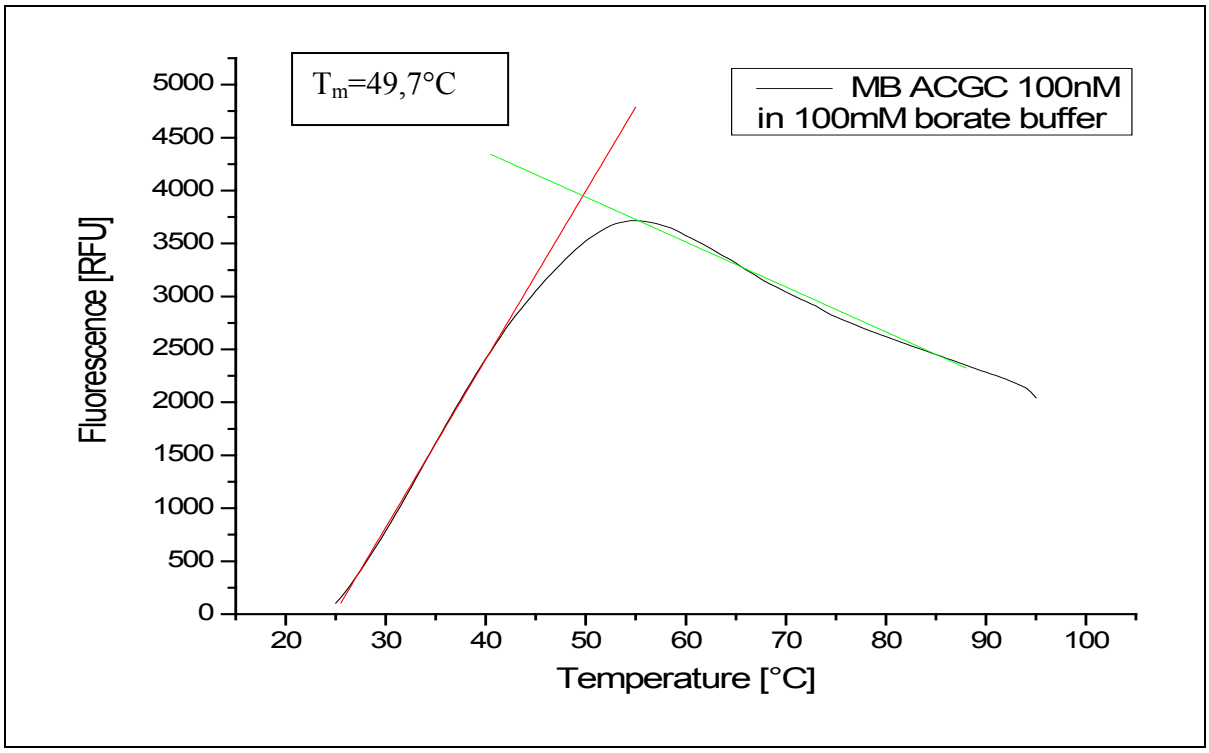

Melting curve III.1.7: 100nM MB ACGC in 100mM bb

tangents: y = 158x - 3940 and y = -42,4x + 6060; resulting Tm=49,7°C

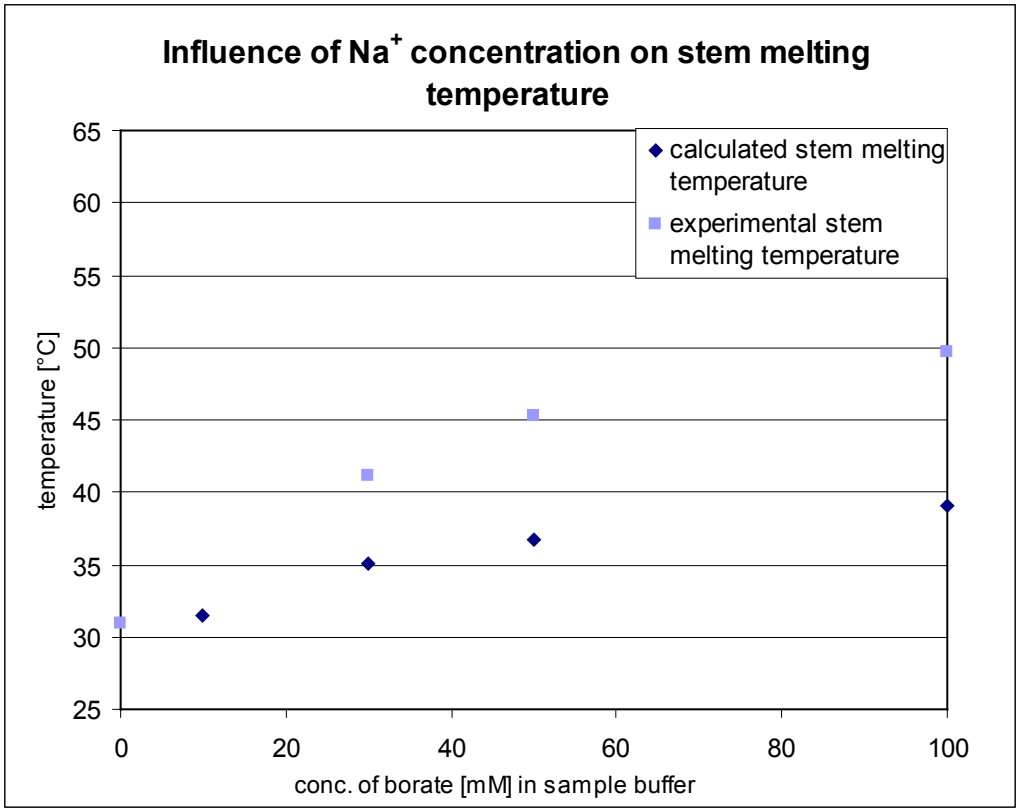

Figure III.1.2: Calculated (with T_m-server by Zuker) and experimental values for the stem melting temperature of the MB ACGC for different sample buffer concentrations.

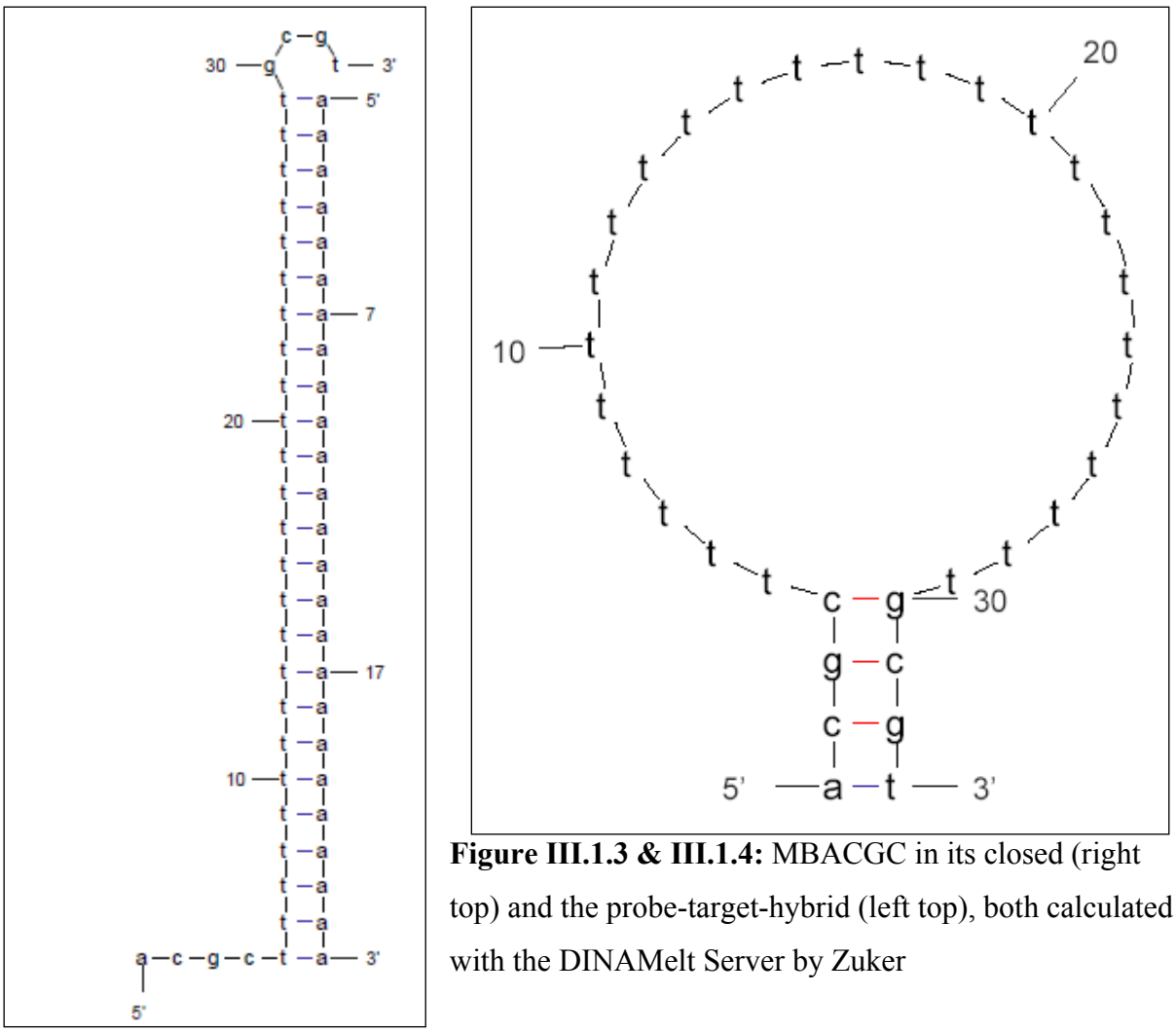

Figure III.1.3 & III.1.4: MBACGC in its closed (right top) and the probe-target-hybrid (left top), both calculated with the DINAMelt Server by Zuker

The melting experiments revealed that the melting properties of the present MB ACGC differ widely from the calculated values. This means that the MB ACGC is more stable in its hairpin-structure than expected. Therefore the method had to be applied according to the recent experimental insight.

Because of the importance of a certain concentration of $MgCl_2$ for forming stable hybrids (Tyagi and Kramer 1996; Bonnet, Tyagi et al. 1999) it was decided to maintain in batch experiments and CE studies with 1,00mM $MgCl_2$. The sample buffer concentration was chosen to be 30mM borate buffer, in order to have a low salt concentration and therefore a lower T_m but sufficient buffer capacity.

III.2 Opening, digestion and hybridization experiments

After the successful characterization of the MB the opening, digestion and hybridization experiments were done to check the highest possible increase of fluorescence signal and if the MB really binds to its target sequence and starts fluorescing. To get the maximum fluorescence signal from the MB ACGC two different methods were used: digestion with DNase I and complexation with ethylenediaminetetraacetic acid (EDTA).
DNase I is a nuclease, an enzyme that digests single- as well as double-stranded DNA and forms DNA fragments. The treatment of the MB ACGC with DNase I would therefore destroy the stem of the Beacon and form smaller oligonucleotides. As result the fluorescent dye would be free in solution and shine brightly. Only quencher molecules which are also free in solution and come close to the fluorophore would cause quenching due to FRET.
EDTA is a very common and useful complexing agent. Added to the MB ACGC it would force the Beacon to undergo a conformational change from its closed to its opened state (see Figure I.2.2, transition from S2 to S3) due to complexation. The fluorescent dye and the quencher would be separated like by thermal denaturation but without rising the temperature and therefore without causing heat induced quenching. Because the dye- and the quencher-moiety are still linked to the DNA strand but separated and in fixed positions not even FRET should occur. The resulting fluorescence increase due to complexation should therefore be higher than due to digestion with DNase.
The in batch hybridization experiments of the MB ACGC with HRV 2 should ensure that the principle of probe-target-hybridization really works and check how large the fluorescent increase would be compared to the digestion and opening experiments.

The digestion experiments of the MB ACGC with DNase I, show a total digestion of the Beacon after 15min at 37°C and a 4,6fold increase of fluorescence (Table III.2.1 & III.2.2). The highest increase of fluorescence was achieved with EDTA. Opening experiments with different concentrations of EDTA led to 6,5fold increase of the fluorescence signal, highest increase was achieved with 1mM and 100nM EDTA (Table V.5.1). Concentrations of EDTA lower than 0,10mM lead to a smaller increase of fluorescence whereas higher concentrations of EDTA above 1,00mM do not lead to any increase of the fluorescent signal at all.
Enhancement of fluorescence was also achieved by incubation with the HRV2. The fluorescent signal of the probe-target hybrid was almost 5 times higher than the signal of the MB without its target under same reaction conditions (Table III.2.1). The hybridization

experiments with poly-a 20 and 80 did not lead to any increase of the fluorescence signal at all.

The data of the digestion, opening and in batch hybridization experiments fit quite well together and suggest that the maximum reachable fluorescent signal is around 5 times higher than its ground signal. Although a 10-20fold increase of the fluorescence signal due to literature (Tyagi and Kramer 1996; Tan, Fang et al. 2000; Browne 2005) was expected the MB probe seemed to work.

Contrary to that the hybridization experiments with our simple, artificial target poly-a failed totally as well as with the in vitro RNA. The lack of any increase of the fluorescent signal due to hybridization with the Poly-a might have two reasons. First reason could be that the MB ACGC hybridizes with the Poly-A but is quenched due to inter-MB quenching (Angelatos, Johnston et al. 2007). The fluorophore of one MB is separated from the quencher, but still in close proximity to the quenching moiety of another MB, probably hybridized to the same Poly-A tail, if it is long enough or to another target sequence. The second reason might be that the MB does not open at all, because the artificial poly-A does not have any rigid, secondary structure, which would force the Beacon to open. The Beacon could hybridize to the poly-A partially without undergoing any conformational change and therefore remaining dark.

But if the fluorescent dye and the quenching moiety are seperated like in the first case, quenching only can occur due to FRET but not due to contact quenching (Marras 2006; Marras 2008). Because FRET is less efficient than contact quenching at least a small enhancement of fluorescence should be noticed. Because of the missing of any increase of the fluorescence signal the second reason becomes more favourable.

Hybridization experiments with the in vitro RNA failed, perhaps the RNA was contaminated and/or already digested by RNase.

Also some in batch hybridization experiments with different preparations of the HRV2 led to no significant increase of the fluorescence signal. It is believed that in some cases despite very careful working the sample was contaminated with RNase and the viral RNA already was digested.

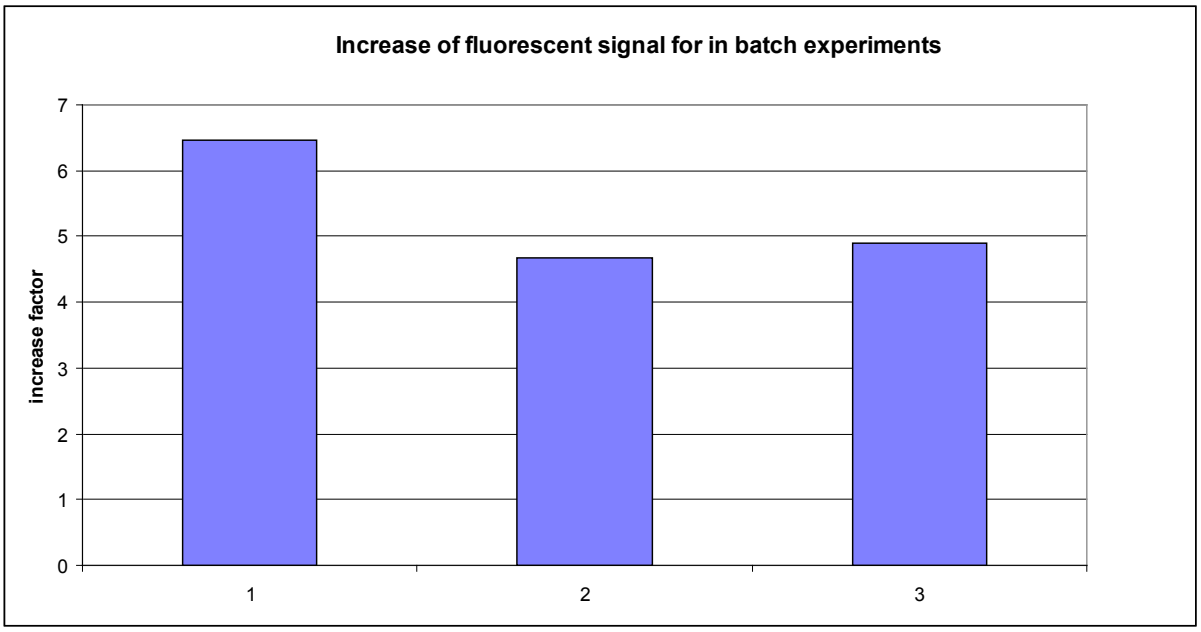

Table III.2.1: increase of the fluorescent signal for in bach experiments; 1) MB ACGC (100nM) + 1mM EDTA; 2): MB ACGC (100nM) + DNase I incubated for 15min at 37°C, measured at 25°C; 3) HRV2 + MB ACGC (100nM) incubated for 15min at 56°C, measured at 25°C; The increase of fluorescence of each method is related to its own negative control. The sample buffer was in all cases 30,00mM bb with 1,00mM $MgCl_2$.

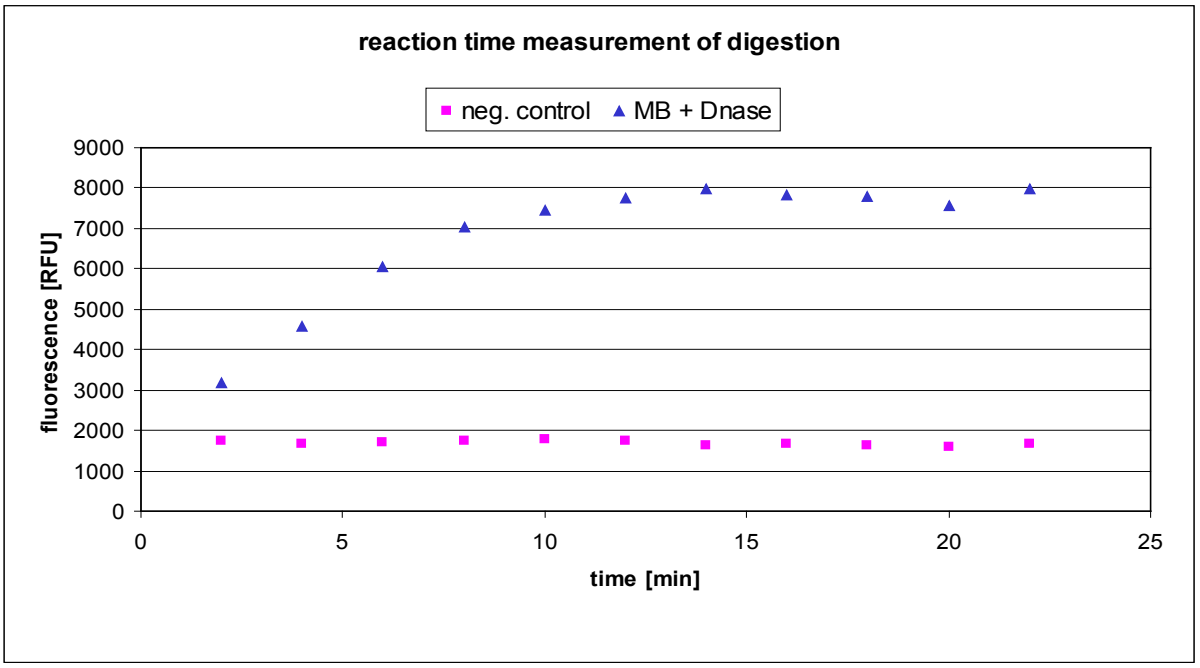

Table III.2.2: reaction time measurement of the MB ACGC; blue: 100nM MB ACGC + DNase I at 37°C, SB: 30mM bb with 1,00mM $MgCl_2$; pink: 100nM MB ACGC without DNase I at 37°C, SB: 30mM bb with 1,00mM $MgCl_2$

III.3 Capillary Electrophoresis experiments

After characterization of the MB ACGC was done and the opening, digestion and hybridization experiments had proved that the Beacon worked efficiently in batch, the next step was to analyse the present MB probe by the aid of capillary electrophoresis. Since the in batch hybridization experiments with our artificial target Poly-A and the in vitro RNA failed, we could not prove that the MB ACGC really binds to its target sequence. Although hybridization of the Beacon with other compounds of the HRV2 like one of the four virus proteins is unlike, it could however not be excluded. Therefore it was necessary to separate the virus proteins from the viral RNA on the CE.

The developed method for CE studies of the MB ACGC based on previous studies of our group (Weiss, Kolivoska et al. 2007; Kremser, Blaas et al. 2009) and was modified according to the insights derived from the characterization of the MB.

The CE results for the HRV2 show that the developed method works efficiently. The buffer capacity with 30mM borate buffer at pH 8.3 as background electrolyte is sufficient, obtained electropherograms and the resulting effective mobilities for each species are totally reproducible. Baseline separation of the virus proteins and the viral RNA is achieved without any additional detergent like sodium dodecyl sulphate (SDS). The EOF has an effective mobility of $69{,}7*10^{-9}$ $m^2/V*s$ and shows up after two minutes shortly before the native HRV2. Due to denaturation the viral RNA is released and the viral capsid decomposes into its four virus proteins. The viral RNA gives a broad peak after 5 minutes with an effective mobility around $-35*10^{-9}$ $m^2/V*s$. The MB ACGC has an effective mobility of $-42*10^{-9}$ $m^2/V*s$ and gives Gaussian shaped peak after 13 minutes. The electrophoretic profile of the denaturated HRV2 and the continous UV-spectra of its compunds and the EOF-marker can be seen in figure III.3.1, the profile of the native HRV2 and the MB ACGC can be seen in electropherogram III.3.1 and III.3.2.

species	μ_{eff}
native HRV2	$-10*10^{-9}$ m^2/Vs
viral RNA	$-35*10^{-9}$ m^2/Vs
Poly-Adenine	$-47*10^{-9}$ m^2/Vs
Cy5	$-19*10^{-9}$ m^2/Vs
MB ACGC	$-42*10^{-9}$ m^2/Vs
EOF	$69*10^{-9}$ m^2/Vs

Table III.3.1: effective mobilities of different species

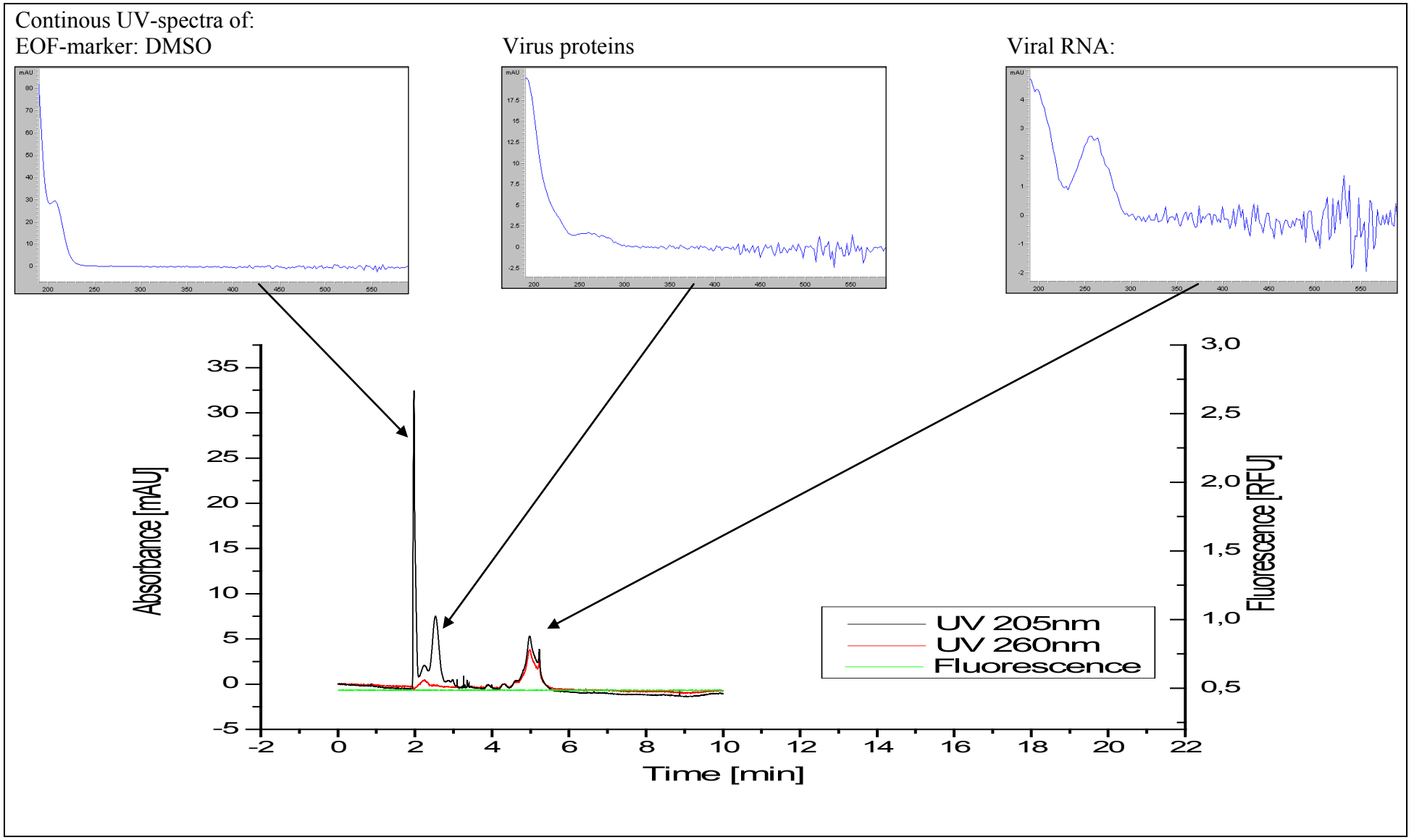

Figure III.3.1: profile of the denaturated HRV2 with EOF marker

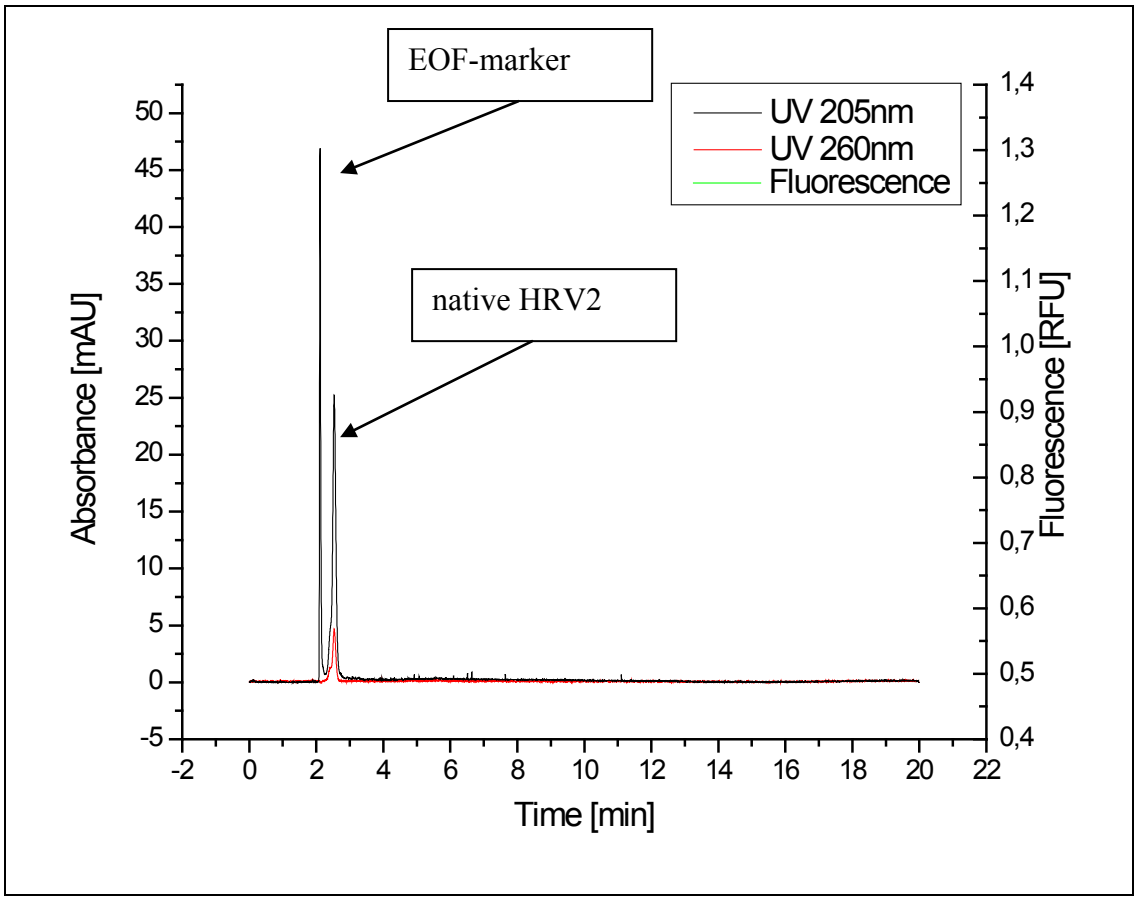

Electropherogram III.3.1: profile of the native HRV2 with EOF-marker

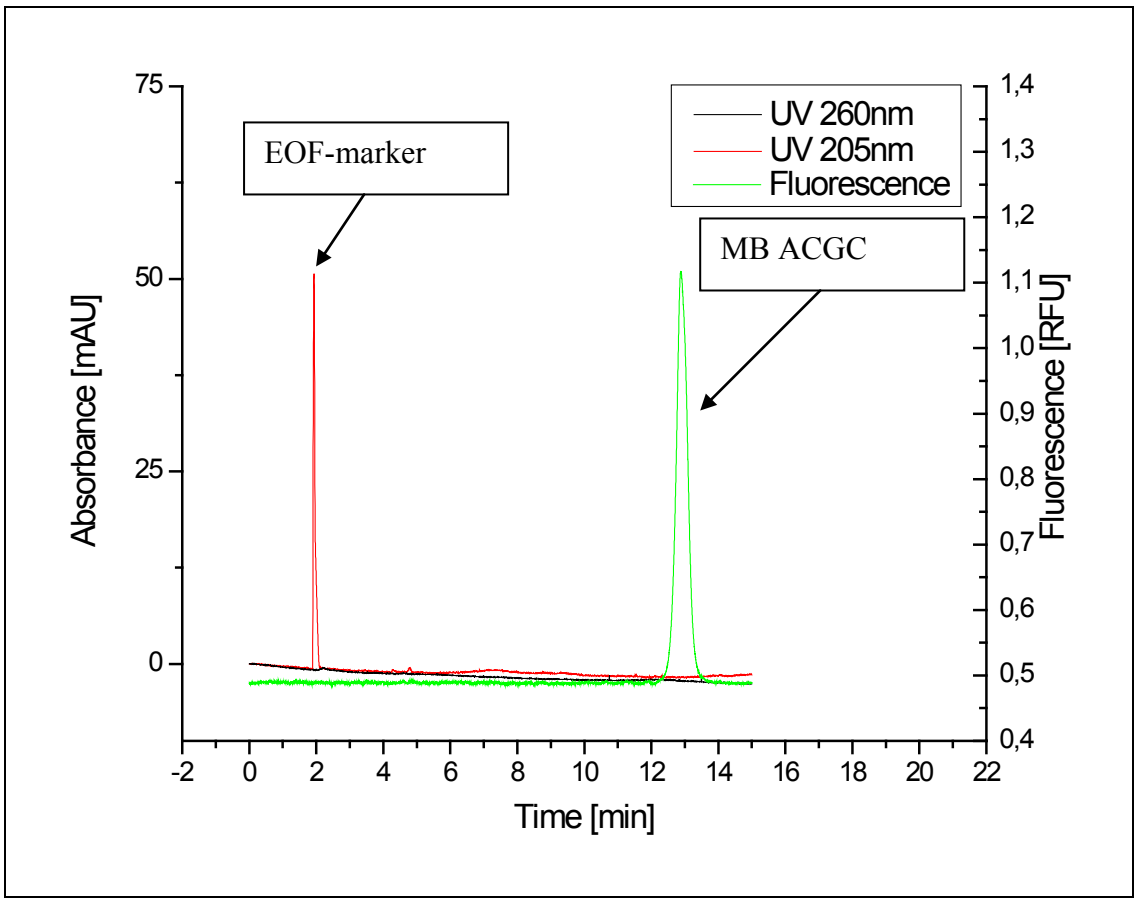

Electropherogram III.3.2: profile of the Molecular Beacon ACGC with EOF marker

III.3.1 Hybridization by Capillary Electrophoresis

Since in batch experiments were successful and the CE method worked efficiently for the analysis of virus and MB, the next step was to separate the probe-target-hybrid. First hybridization of the MB ACGC with the artificial target Poly-A was tried. Since the in batch experiments with the Poly-A were not successful, we wanted to know what the reason for this was.

The hybridization experiments with the artificial target Poly-a on the CE neither show a change of the signal intensity nor of the effective mobility of one of the two supposed reaction partners (see electropherogram III.3.3). Theses results confirm the results of the in batch experiments with Poly-A and the MB. But the fact that the effective mobility of the MB and the Poly-A are different, indicate that there is no hybridization at all.

The next step was the hybridization of the MB ACGC with viral RNA of the HRV2 and its separation to get clear evidence that the Beacon really binds to its target.

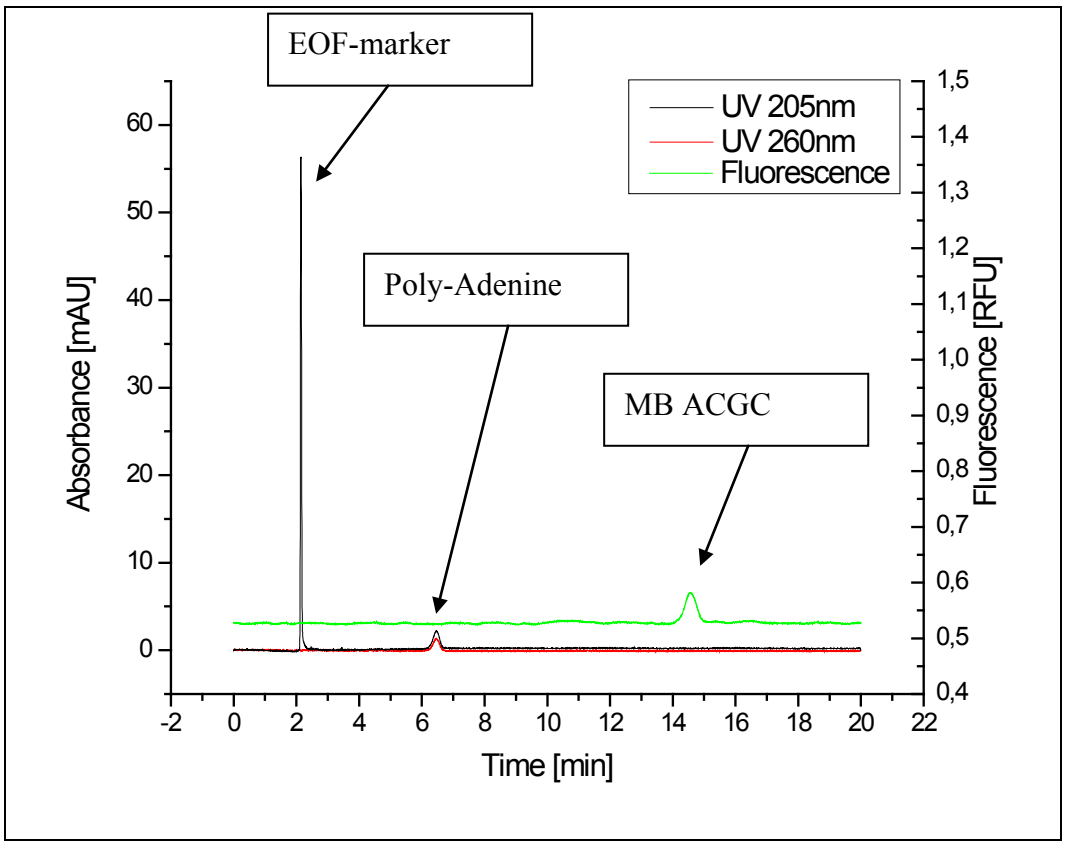

Electropherogram III.3.3: MB ACGC with the artificial target Poly-a and EOF-marker

The hybridization experiments of the MB ACGC and the denaturated HRV2 give some interesting results. Indeed the hybridization experiments lead to additional signals with a much higher intensity and a different effective mobility than the signal of the closed Beacon. In some experiments even a 100fold increase of fluorescence was detected. But number, intensities and effective mobilities of these additional signals differ strongly from one to another sample, despite equal sample preparation. Nevertheless a correlation between the different results can be seen, because additional fluorescence signals mainly appear in two different mobility windows.

On the one hand we obtain a large number of signals with different signal intensities (see electropherogram III.3.4 and V.3.4), which effective mobilities are located in between $-31*10^{-9}$ $m^2/V*s$ and $-37*10^{-9}$ $m^2/V*s$ and are therefore exactly around the effective mobility of viral RNA ($-35*10^{-9}$ $m^2/V*s$). This indicates that the MB is hybridized to its target the viral RNA.

On the other hand we derive single peaks of high intensity (see electropherogram III.3.5; V.3.3 & V.3.5) with effective mobilities ranging from $-23*10^{-9}$ $m^2/V*s$ up to $-30*10^{-9}$ $m^2/V*s$ with corresponding signals of same mobility in the UV. Though the mobilities of these signals do not match with those of the viral RNA, the spectra of the corresponding UV signals show clearly that there is some viral RNA. Taking this into account it leads to the assumption that probe-target hybrids are formed but co-migrate with the virus proteins.

But all these signals hold some immanent enervation. The shape of all these suspected hybrid signals is by far too sharp, in some cases the peaks are less than a second broad. Compared to the Gaussian like signal of the closed MB ACGC, the signal of the fluorescent dye Cy5 or the signals of the fragments of the digested MB this is unexpected and also very unlikely. Though to the significant high signal intensities compared to the closed MB , the very sharpness of these peaks hampers evaluating them by integration. Whereas the signal of the closed Beacon and its in- or decrease can be evaluated very well. And in fact as soon as the suspected, sharp hybridization signals appear the signal of the closed MB ACGC decreases, in some cases down to 20% of the original signal.

But the biggest handicap of these results is probably their low reproducibility. 60% of all capillary electrophoresis measurements do not show any suspected probe-target signals and/or a decrease of the closed MB signal.

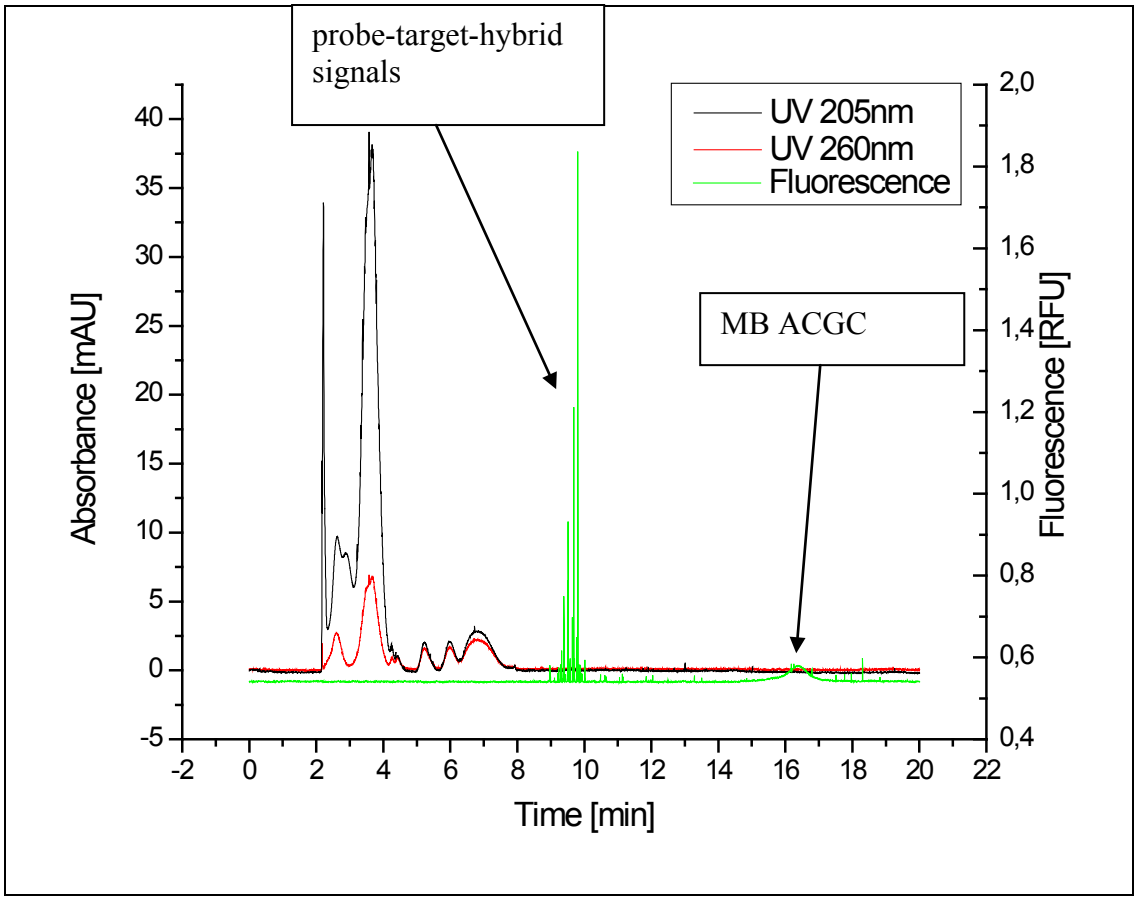

Electropherogram III.3.4: MB ACGC with denaturated HRV2 and EOF-marker

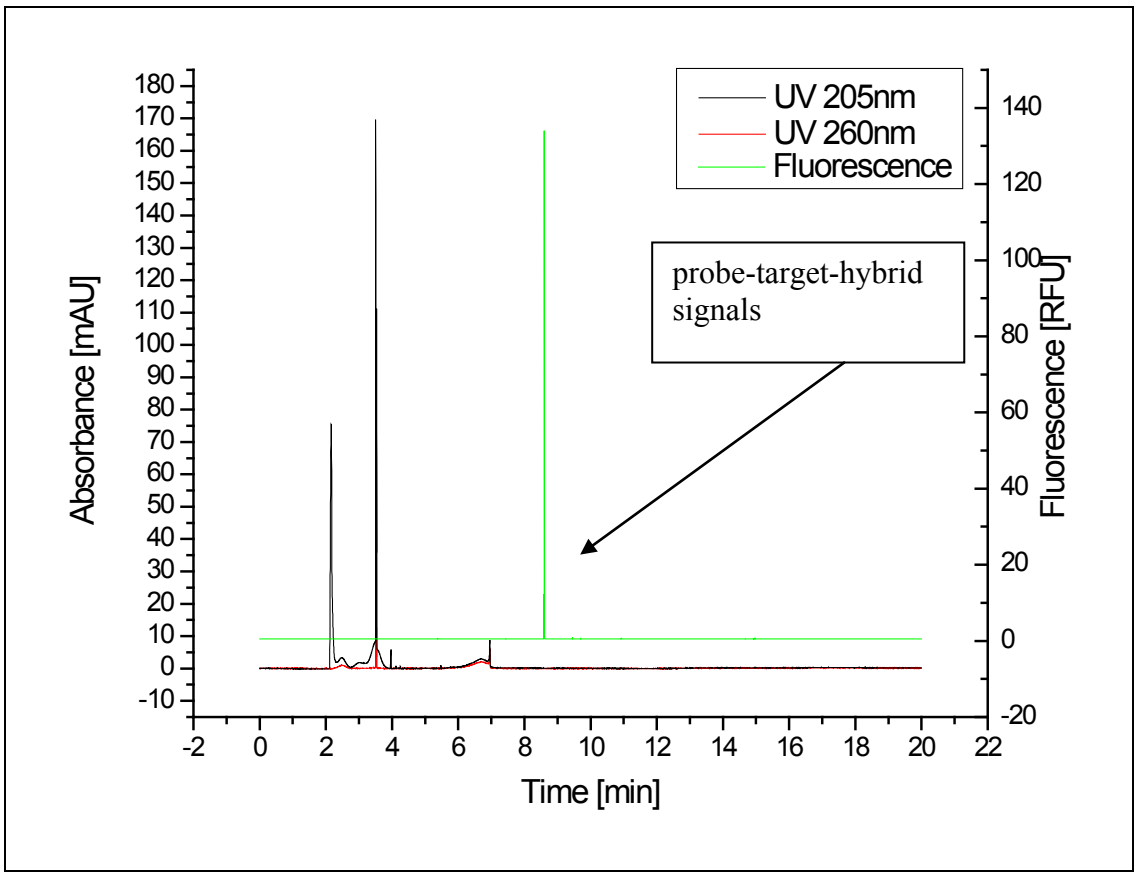

Electropherogram III.3.5: MB ACGC with denaturated HRV2 and EOF-marker

IV. Conclusions

The Characterization of the MB showed clearly that the salt concentration in the sample buffer in general and the concentration of $MgCl_2$ in special have a large influence on the stem melting temperature of the MB ACGC and that the free available T_m server by Zuker for calculating such stem melting temperatures underestimates this influence. Only calculations for minimum salt concentrations in the sample buffer without $MgCl_2$ seem to be consistent with experimental data. For the correct design of a MB in future it is advisable to use additional programs for Beacon design and calculation of melting properties like Beacon Designer ™ (PREMIER Biosoft International).

The test system for hybridization of the MB ACGC with the artificial Poly-A did not work. The in batch and CE results indicate in contrast to previous calculations with the 2-state-hybridization server by Zuker that there is no formation of a probe-target-hybrid at all. I assume that the existence of a rigid, secondary structure of the target is immanent for successful probe-target hybridization.

The hybridization experiments of the MB ACGC with the denaturated HRV2 provides contrary results. The in batch experiments prove that the MB opens due to hybridization, resulting up to 6-fold increase of fluorescence. A possible reason for the relatively low increase of fluorescence signal, a double-digit value was expected, may be the limitation of the set-up for in batch experiments consisting of the Perkin Elmer Victor 3 1420 Multilaber Plate Reader. Because the plate reader uses a CW lamp filter for excitation of a fluorescent dye the fluorescence yield is probably lower than excitation with a monochromatic light source. However we cannot quantify the influence of different light sources for excitation. An other reason which we cannot exclude totally, though accurate consideration is the choice of our fluorophore-quencher-pair Cy5 and BHQ.

CE experiments indicate the formation of a hybrid between the MB ACGC and the viral RNA. CE-LIF results show an up to 100fold increase of fluorescence light, which strengthens the assumption that a monochromatic light source for fluorescene excitation is essential for a high yield.

But shape and intensity of these suspected hybrid signals rather remind of system peaks than real sample peaks. But a check for system eigenmobilities, which can cause peaks of abnormal sharpness and intensity reveals no further awareness. A possibility could be the formation of RNA fragments due to denaturation onto which the Beacon hybridizes or fragmentation of the viral RNA after the hybrid was formed. RNA fragments of different

length and therefore slightly different mobilities onto which the probe is hybridized could cause these signals.

But however the CE results are interpreted, the low reproducibility of the experimental data on the CE remains the biggest problem for MB-based studies on CE. A potential way to improve the reproducibility of CE experiments maybe the enhancement of probe-target affinity by choosing a different target sequence than the Poly-A sequence in the viral RNA. Generally the choice of the Poly-A as target sequence for our MB ACGC seems not to be ideal. Calculations with the 2-state-hybridization server by Zuker showed that the affinity of the MB ACGC to its target sequence is sufficient. But taking the wrong presumptions of the melting properties into to account, we have to challenge these calculations. Choosing a different target sequence however could increase the affinity between probe and target significantly.

Despite some weaknesses of this research work, which concern the results of the CE experiments, we could prove that the MB method for recognition of viral RNA works. The main focus for further MB-based studies on CE will be on improving the reproducibility of CE results and their quality.

V. Appendix

V.1. Citations

Angelatos, A. S., A. P. Johnston, et al. (2007). "Probing the permeability of polyelectrolyte multilayer capsules via a molecular beacon approach." Langmuir **23**(8): 4554-62.

Bonnet, G., S. Tyagi, et al. (1999). "Thermodynamic basis of the enhanced specificity of structured DNA probes." Proc Natl Acad Sci U S A **96**(11): 6171-6.

Browne, K. A. (2005). "Sequence-specific, self-reporting hairpin inversion probes." J Am Chem Soc **127**(6): 1989-94.

Drake, T. J. and W. Tan (2004). "Molecular beacon DNA probes and their bioanalytical applications." Appl Spectrosc **58**(9): 269A-280A.

Gerber, K., E. Wimmer, et al. (2001). "Biochemical and genetic studies of the initiation of human rhinovirus 2 RNA replication: purification and enzymatic analysis of the RNA-dependent RNA polymerase 3D(pol)." J Virol **75**(22): 10969-78.

Kostrikis, L. G., S. Tyagi, et al. (1998). "Spectral genotyping of human alleles." Science **279**(5354): 1228-9.

Kremser, L., D. Blaas, et al. (2009). "Virus analysis using electromigration techniques." Electrophoresis **30**(1): 133-40.

Marras, S. A. (2006). "Selection of fluorophore and quencher pairs for fluorescent nucleic acid hybridization probes." Methods Mol Biol **335**: 3-16.

Marras, S. A. (2008). "Interactive fluorophore and quencher pairs for labeling fluorescent nucleic acid hybridization probes." Mol Biotechnol **38**(3): 247-55.

Marras, S. A., F. R. Kramer, et al. (2002). "Efficiencies of fluorescence resonance energy transfer and contact-mediated quenching in oligonucleotide probes." Nucleic Acids Res **30**(21): e122.

Ortiz, E., G. Estrada, et al. (1998). "PNA molecular beacons for rapid detection of PCR amplicons." Mol Cell Probes **12**(4): 219-26.

Prchla, E., E. Kuechler, et al. (1994). "Uncoating of human rhinovirus serotype 2 from late endosomes." J Virol **68**(6): 3713-23.

Tan, W., X. Fang, et al. (2000). "Molecular beacons: a novel DNA probe for nucleic acid and protein studies." Chemistry **6**(7): 1107-11.

Torimura, M., S. Kurata, et al. (2001). "Fluorescence-quenching phenomenon by photoinduced electron transfer between a fluorescent dye and a nucleotide base." Anal Sci **17**(1): 155-60.

Tyagi, S., D. P. Bratu, et al. (1998). "Multicolor molecular beacons for allele discrimination." Nat Biotechnol **16**(1): 49-53.

Tyagi, S. and F. R. Kramer (1996). "Molecular beacons: probes that fluoresce upon hybridization." Nat Biotechnol **14**(3): 303-8.

Verdaguer, N., D. Blaas, et al. (2000). "Structure of human rhinovirus serotype 2 (HRV2)." J Mol Biol **300**(5): 1179-94.

Weiss, V. U., V. Kolivoska, et al. (2007). "Virus analysis by electrophoresis on a microfluidic chip." J Chromatogr B Analyt Technol Biomed Life Sci **860**(2): 173-9.

"Structure-based Study of Viral Replication", edited by R Holland Cheng (University of California, Davis, USA) & Tatsuo Miyamura (The National Institute of Infectious Disease, Japan)

V.2 Melting Curves

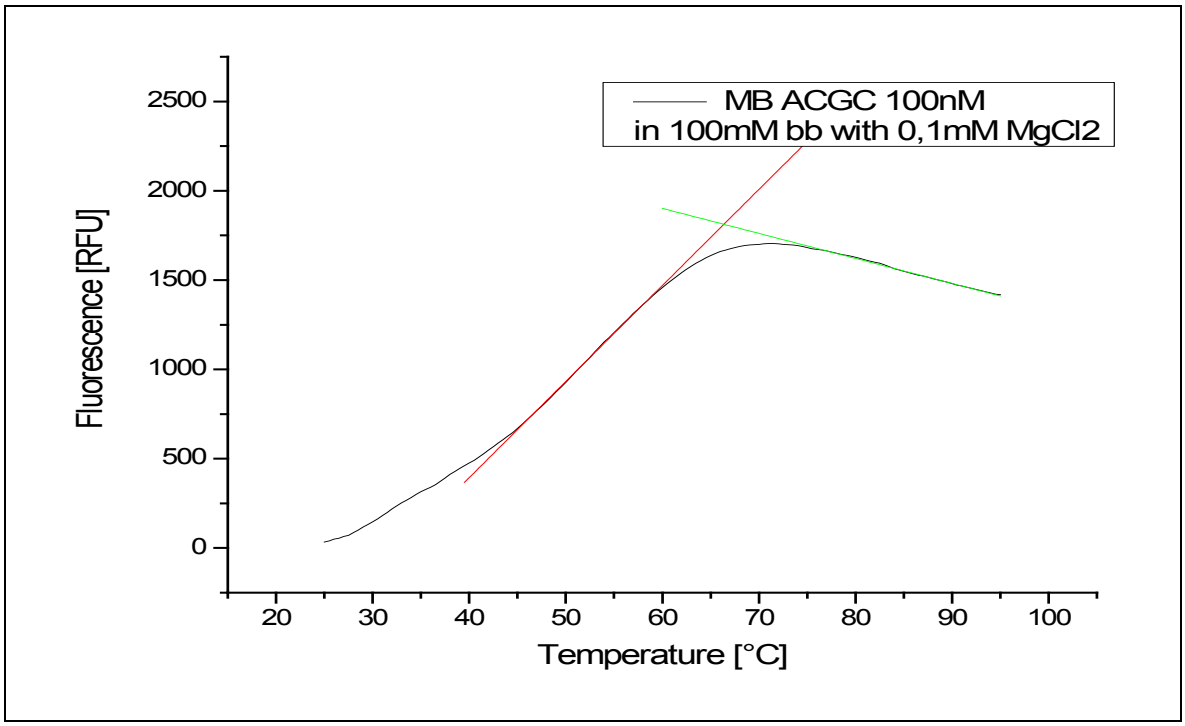

Melting curve V.2.1: tangents: y = 53,792 - 1757,7 and y = -14,001x + 2742,4 resulting Tm=66,38°C for 100nM MB ACGC in 100mM bb with 0,10mM $MgCl_2$

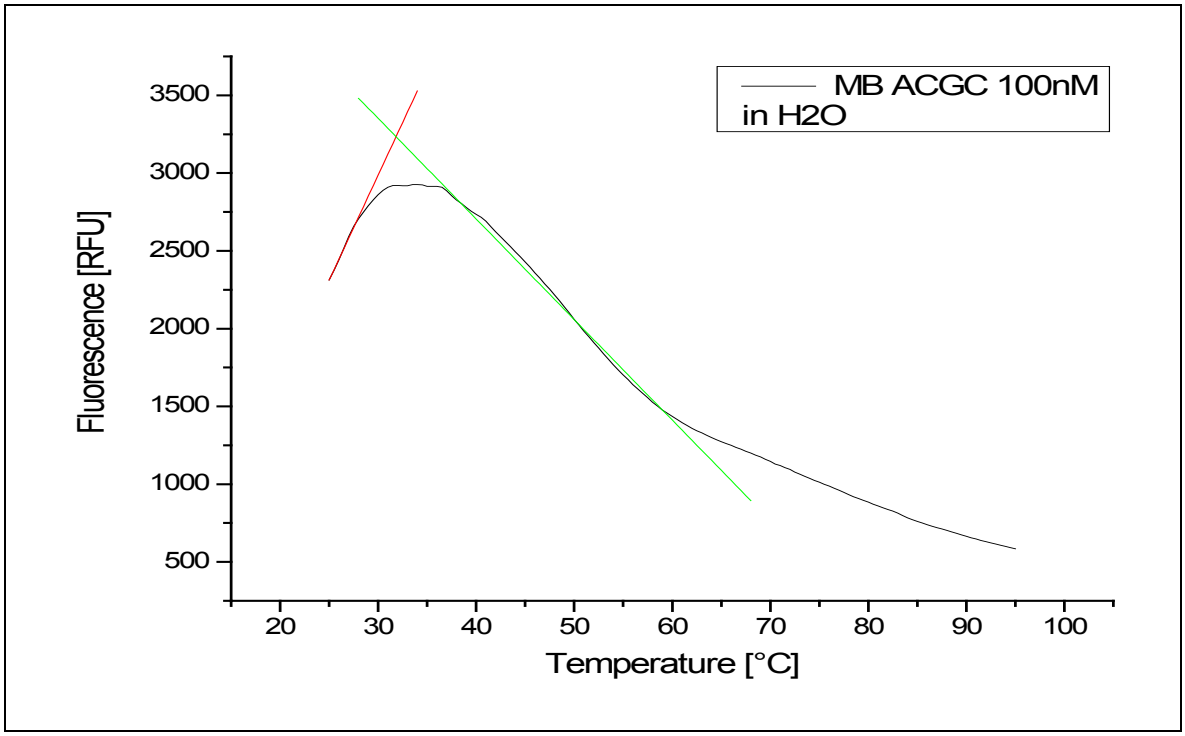

Melting curve V.2.2: tangents: y = 135,21x - 1068,3 and y = -64,655x + 5291,3 resulting Tm=31,82°C for 100nM MB ACGC in H_2O

V.3 Electropherograms

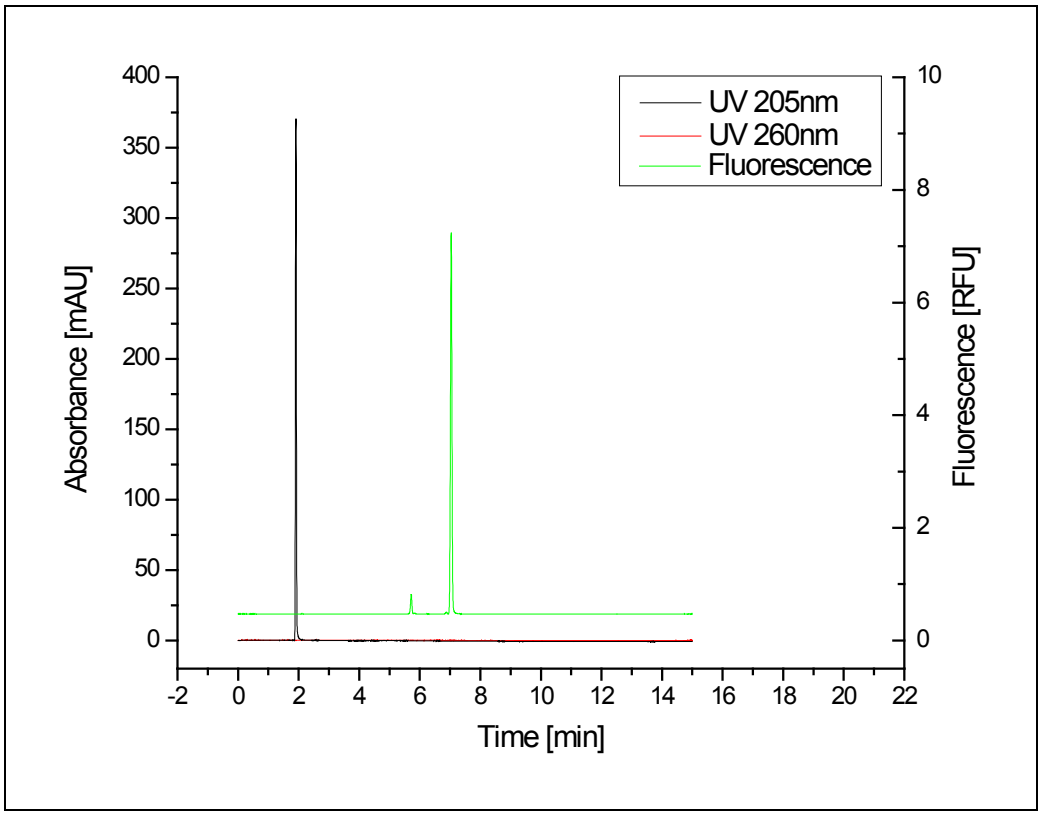

Electropherogram V.3.1: Cy5 with EOF marker

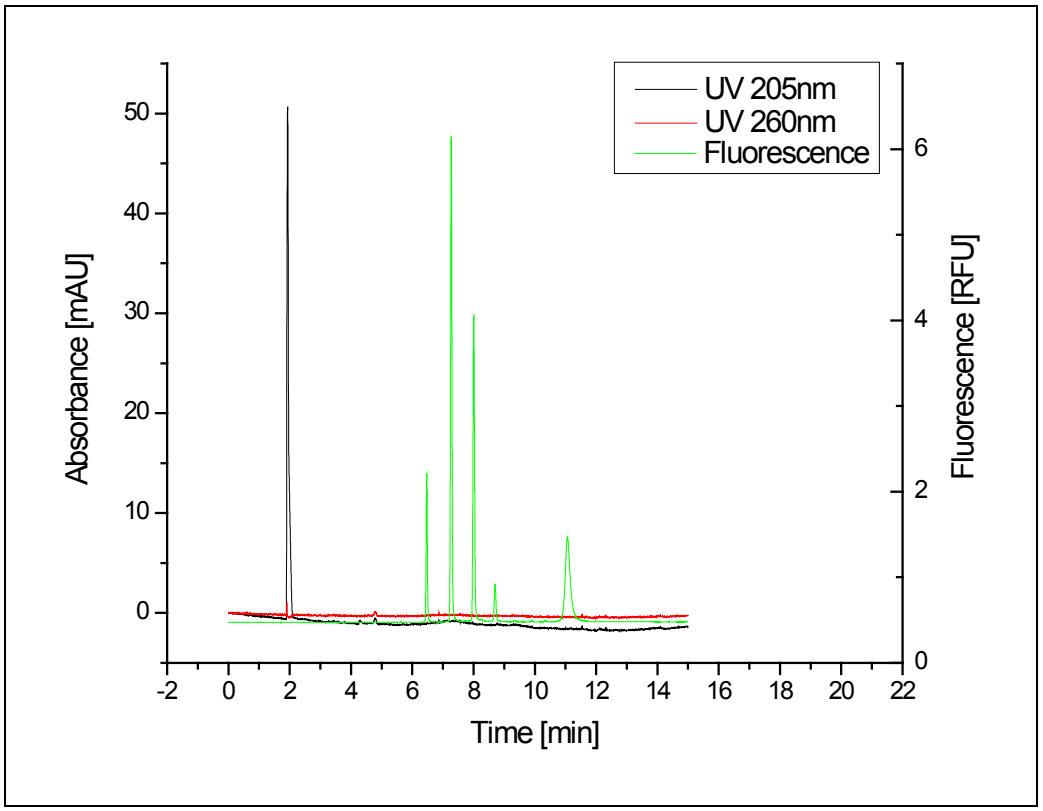

Electropherogram V.3.2: profile of the digested MB ACGC (with DNase I) with EOF marker

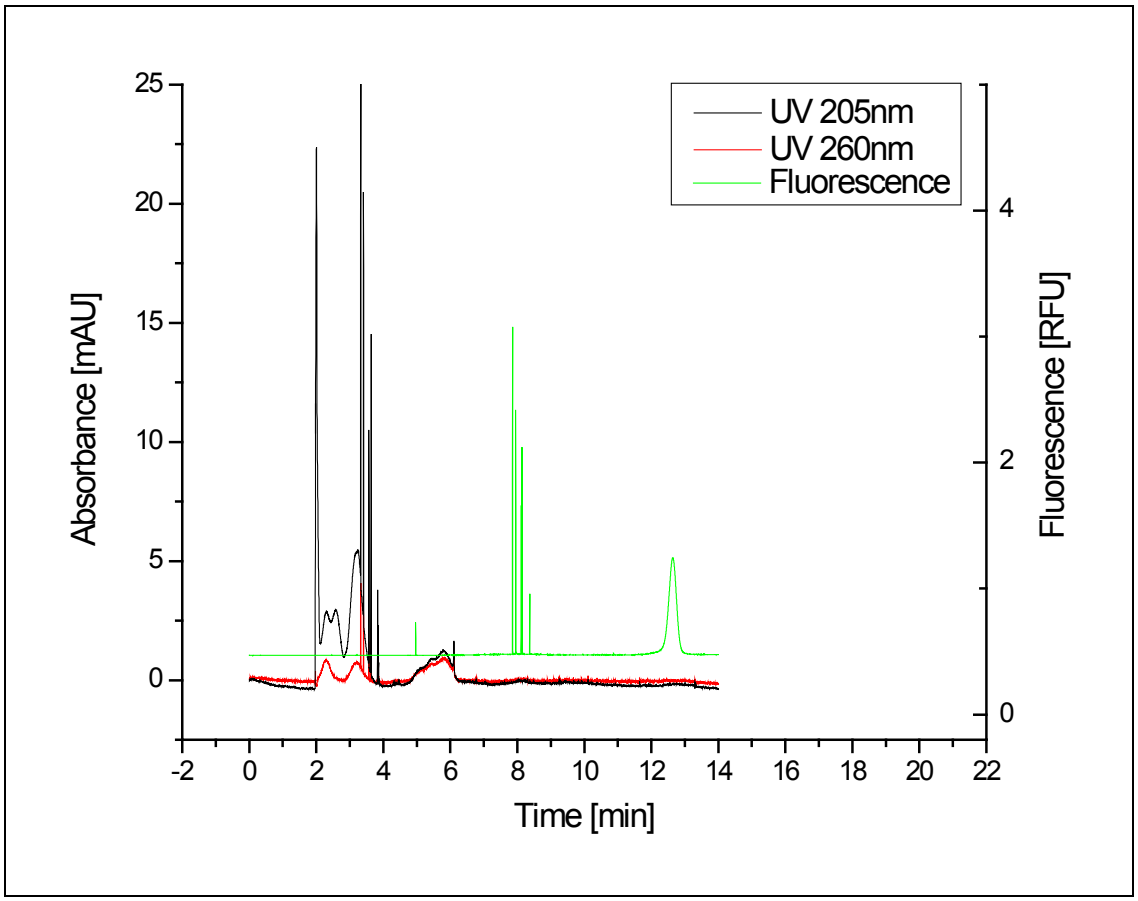

Electropherogram V.3.3: MB ACGC with denaturated HRV2 and EOF-marker

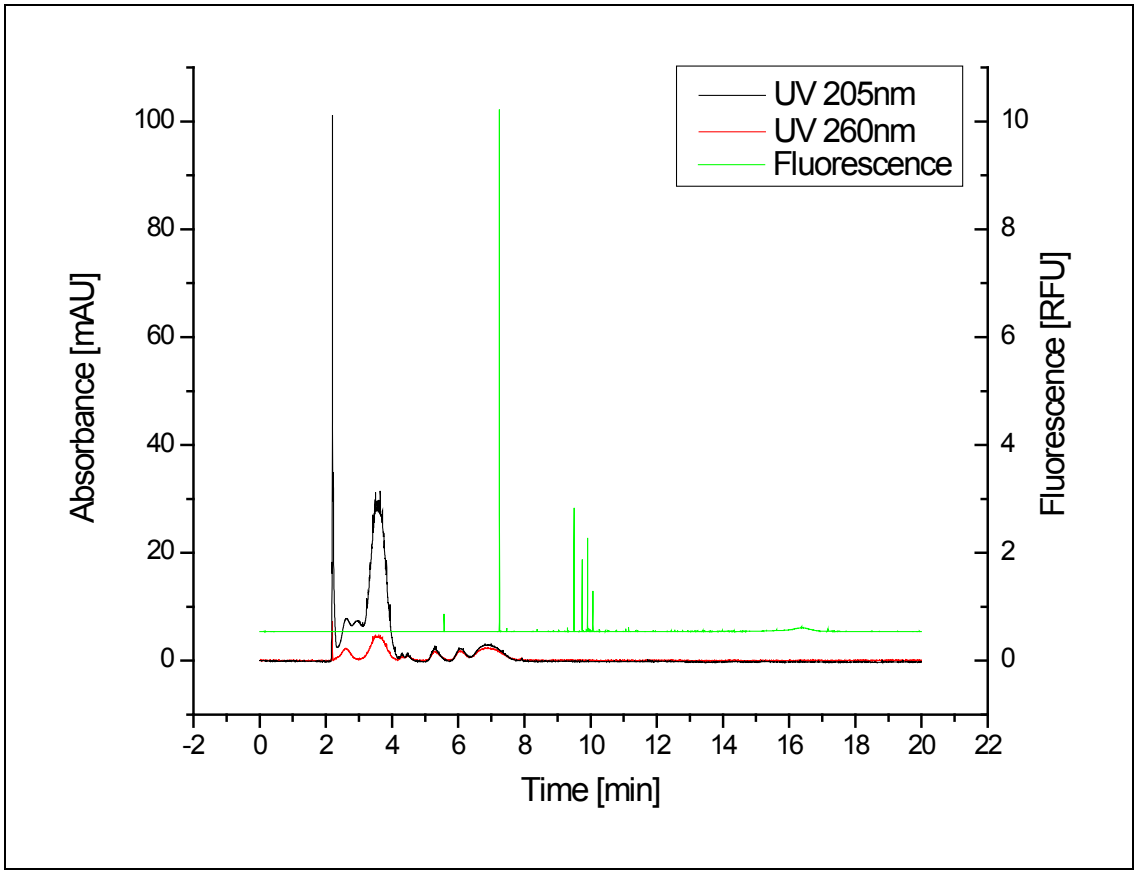

Electropherogram V.3.4: MB ACGC with denaturated HRV2 and EOF-marker

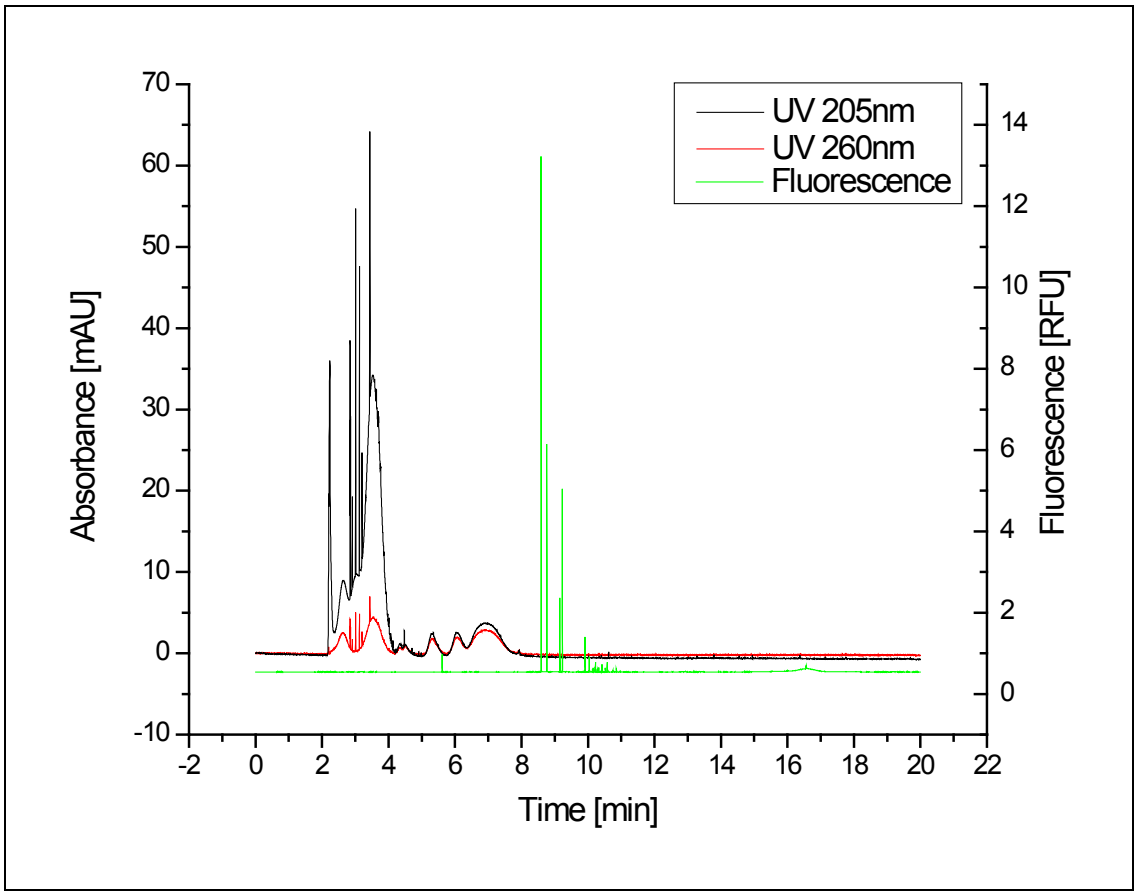

Electropherogram V.3.5: MB ACGC with denaturated HRV2 and EOF-marker

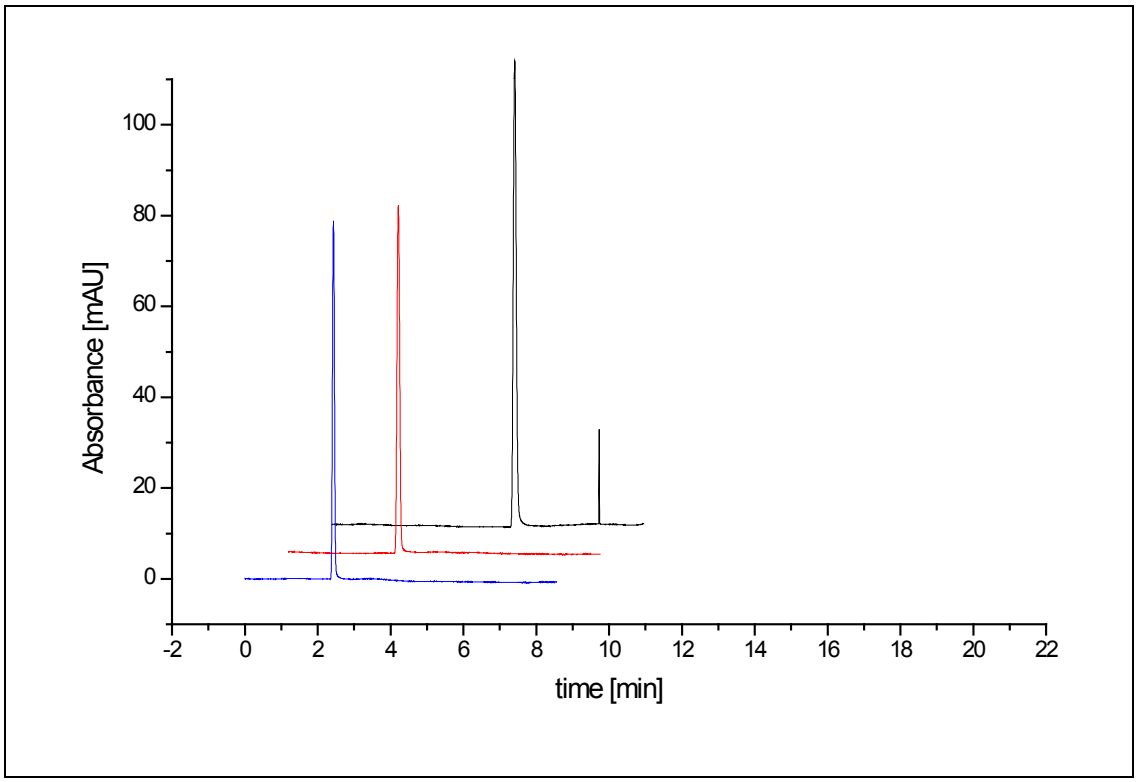

Electropherogram V.3.6: Unreproducible change of the EOF by using $MgCl_2$ in the BGE

V.4 Incubation and Opening experiments

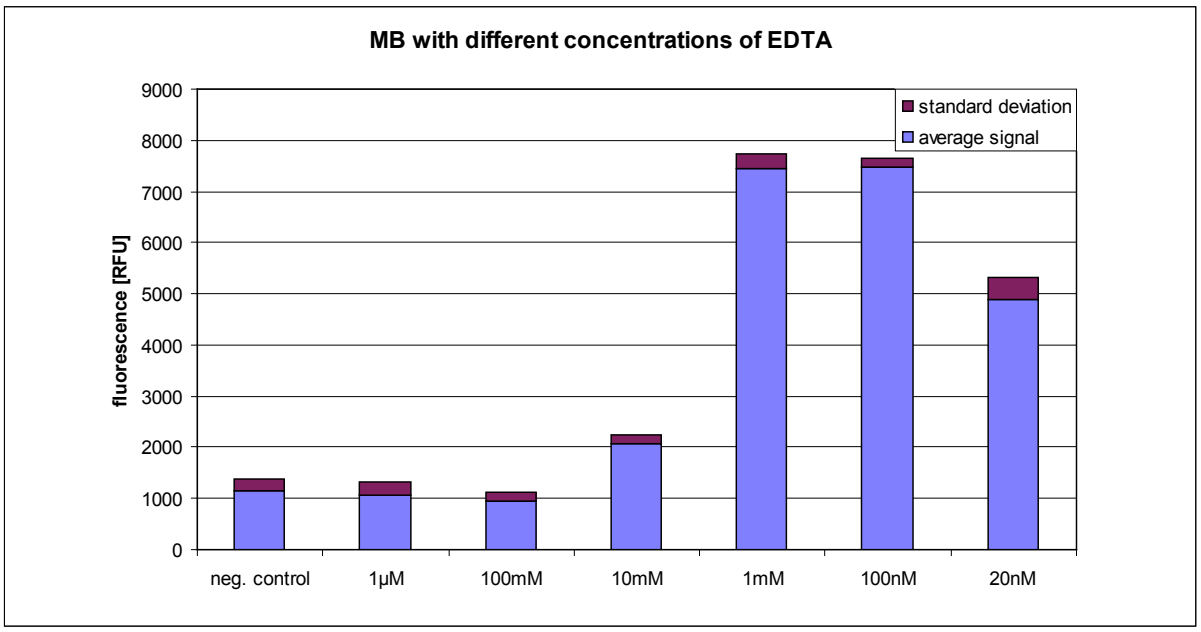

Table V.4.1: opening experiments of the MB ACGC with different concentrations of EDTA

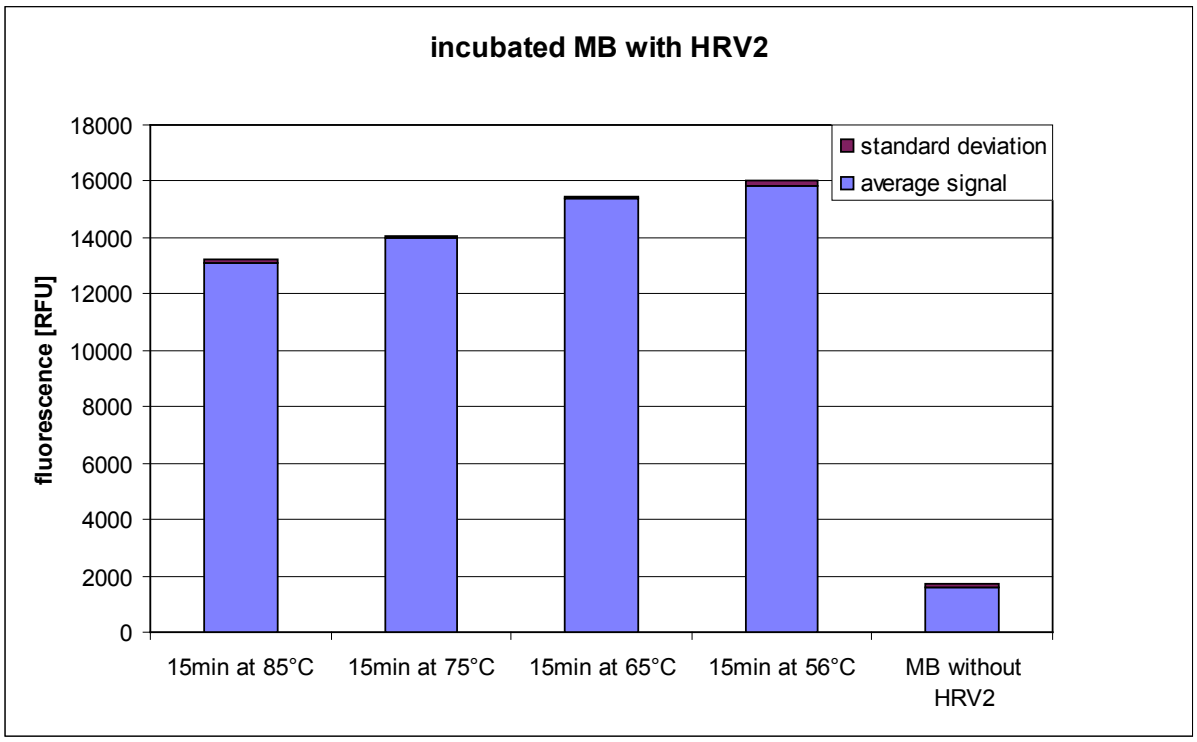

Table V.4.1: Hybridization experiments of the MB ACGC with HRV2 at different temperatures

List of abbreviations				
k_e	electric force		BHQ	Black Hole Quencher
z	charging number		CE	Capillary electrophoresis
c_{corr}	correction factor		CW	Continous Wavelength
E	electric field strength		DMSO	Dimethylsulfoxide
k_η	friction force		DNA	Desoxyribonucleic Acid
$\mu_{i,0}$	absolute mobility		DNase	Desoxyribonuclease
$\mu_{i,act}$	actual mobility		EDTA	Ethyldiamintetraacetate
$\mu_{i,eff}$	effective mobility		FRET	Fluorescence Resonance Energy Transfer
ν	velocity		HRV	Human Rhinovirus
η	dynamic viscosity		ICAM	Intercellular Adhesion Molecule
f	friction coefficient		LDL	Low Density Lipoprotein
κ_i	conductivity		LIF	Laser Induced Fluoresence
ε_0	vacuum permittivity		MB	Molecular Beacon
ε_r	permittivity of water at 25°C		RNA	Ribonucleic Acid
ζ	zeta-potential		RNase	Ribonuclease
α_i	dissociation coefficient		T_m	Melting Temperature
λ_i	molar conductivity		VP	Virus Protein
T	temperature			
I	ionic strength			
k	Boltzmann constant			
e	elementary charge of an electron			
γ_i	activity coefficient			

Abstract

The present work deals with a new method for DNA/ RNA recognition, the Molecular Beacon probe. A Molecular Beacon is able to recognize and bind to a specific DNA or RNA target sequence. Due to this hybridization of the probe and the target, the Beacon undergoes a conformational change and starts fluorescing.

The aim of this scientific project was to design a Molecular Beacon probe that is able to hybridize upon viral RNA of the Human Rhinovirus 2 and to apply this method for virus analysis by capillary electrophoresis. Human Rhinoviruses are the pathogen agent for the common cold in the human body and therefore the cause for one of the most frequent infections at all.

Design, characterization and application of the Molecular Beacon ACGC for viral RNA recognition are described. Melting experiments reveal a strong influence of Mg^{2+} and a smaller influence of Na^{+} concentration on melting properties of the Molecular Beacon. In batch experiments prove that the Molecular Beacon opens due to hybridization, resulting in up to 6-fold increase of fluorescence. Results of Capillary Electrophoresis experiments with Laser Induced Fluorescence detection even show an up to 100fold increase of fluorescence light for the probe-target-hybrid.

Despite some weaknesses of this method it could be shown that this novel tool for bioanalytical chemistry works, but further investigations to improve the reliability of this method especially for capillary electrophoresis experiments have to be done.